Received 4 May 2024; accepted 28 May 2024. Date of publication 3 June 2024; date of current version 24 June 2024.
Digital Object Identifier 10.1109/OJCOMS.2024.3408313

Performance of Full-Duplex Cooperative NOMA Network With Direct Link and Battery-Assisted Non-Linear Energy Harvesting Near User

MUDASIR BAKSHI [1] (Graduate Student Member, IEEE), BREJESH LALL [2] (Senior Member, IEEE), RANJAN K. MALLIK [2] (Fellow, IEEE), AND AMIT SINGHAL [3] (Senior Member, IEEE)

[1]Bharti School of Telecommunication Technology and Management, Indian Institute of Technology Delhi, New Delhi 110016, India
[2]Department of Electrical Engineering, Indian Institute of Technology Delhi, New Delhi 110016, India
[3]Department of Electronics and Communication Engineering, Netaji Subhas University of Technology, New Delhi 110078, India
CORRESPONDING AUTHOR: M. BAKSHI (e-mail: bsz188117@iitd.ac.in)

The work of Ranjan K. Mallik was supported in part by the Science and Engineering Research Board, a Statutory Body of the Department of Science and Technology, Government of India, under the J. C. Bose Fellowship.

ABSTRACT This study investigates the performance of cooperative relaying-based non-orthogonal multiple access (NOMA) with simultaneous wireless information and power transfer. Assuming the battery-assisted non-linear energy harvesting (NL-EH) in which the near user (NU) works as a relay for the far user (FU) to convey data from the base station (BS); two scenarios are examined: (1) No direct link (NDL) between the BS and the FU, and (2) direct link (DL) between the BS and the FU. The DL at the FU is evaluated in two scenarios: as an optimal combination to the signal from the NU and as an interfering link to the signal from the NU. Considering the power splitting relaying (PSR) protocol with an NL-EH model and assuming imperfect successive interference cancellation (i-SIC) at the NU, we derive closed-form expressions for the NU and FU outage probability and throughput. The throughput of the FU is greatly increased by supplementing the harvested energy with a small quantity of battery energy. Furthermore, an optimal combination of the FU signals relayed from the BS and the NU considerably improves the throughput of the FU. It reduces the energy consumption at the battery compared to the scenario when there is NDL. We obtain the diversity order by deriving high signal-to-noise ratio approximations for the NU and FU outage probability in NDL and DL scenarios. Unlike linear energy harvesting, we show NL-EH leads to a loss of diversity, making it even more important to use the DL. We have formulated an equation to measure energy efficiency using the derived throughput expressions for the NDL and DL scenarios. We have also shown that selecting the optimal combination of battery energy and PS parameter is essential to achieve the highest possible throughput and energy efficiency. The residual interference generated by i-SIC significantly impacts the outage probability of the NU while having a negligible effect on the performance of the FU. Moreover, we have discovered that performance deteriorates when interference from the DL is present. We explain how the system's performance is affected by the selection of energy harvesting parameter, power allocation coefficient, saturation threshold, self-loop interference, variable node distances and battery energy. Monte Carlo simulations have verified the accuracy of the resulting expressions.

INDEX TERMS Energy harvesting (EH), non-orthogonal multiple access (NOMA), power-splitting (PS), simultaneous wireless information and power transfer (SWIPT).

I. INTRODUCTION

THE NON-ORTHOGONAL multiple access (NOMA) approach is a new technique that enhances the efficiency of fifth-generation (5G) wireless networks. This technology is becoming increasingly important and promising for these networks [1], [2]. Power domain NOMA provides multiple users with a single resource slot, such as time, frequency, or code [3]. The upcoming wireless networks

© 2024 The Authors. This work is licensed under a Creative Commons Attribution-NonCommercial-NoDerivatives 4.0 License.
For more information, see https://creativecommons.org/licenses/by-nc-nd/4.0/

are expected to deliver high data rates, ensure widespread connectivity, and save energy. Enormous machine-type communication and the Internet of Things (IoT) will require future-generation networks to support low-power machine-type devices (MTDs) with extended battery lives [4], [5]. Harvesting energy from the radio frequency signals to create self-sustaining communication nodes is a viable solution to avoid frequent battery replacements. NOMA and full-duplex (FD) are feasible alternatives for attaining the desired spectrum efficiency goals. The FD method allows simultaneous transmission and reception of signals in the same frequency band, roughly doubling spectral efficiency [6]. On the other hand, NOMA uses power domain multiplexing and successive interference cancellation (SIC) to enable multiple users to share the time, frequency, and code resources [7]. Cooperative relaying effectively enhances the reliability and coverage of NOMA networks [8]. There are two primary categories of cooperative relaying in NOMA. These two categories are relay-assisted NOMA and cooperative NOMA. Within the framework of IoT, the far user (FU) in cooperative NOMA can receive assistance from the near user (NU) in information exchange [9]. Conversely, the information is sent to the FU through a specialized relay in relayed NOMA, while the source links directly to the NU [10]. In a cooperative NOMA framework, the relay operation traditionally utilizes the energy from the NU's battery, significantly reducing its battery life and necessitating frequent battery replacement [11]. Communication nodes that are autonomous, green, and use simultaneous wireless information and power transfer (SWIPT) technology are replacing traditional battery-powered devices. Using SWIPT in cooperative scenarios expands the coverage area while ensuring efficient battery energy use at the relay [12].

The feasibility of SWIPT as a solution to this issue has drawn significant scientific interest. In [13], the research was conducted on two different energy harvesting (EH) studies: power-splitting relaying (PSR) and time-switching relaying (TSR). The received signal is split between EH and information transmission (IT) in PSR. In contrast, a dedicated portion of the signalling period is utilized for EH in TSR. Higher throughput is achieved with power-splitting (PS) but at the cost of more complicated circuitry [14], although time-switching (TS) is more energy-efficient [15] in certain situations.

A. LITERATURE SURVEY

Spectral and energy efficiency can be significantly improved by integrating self-sustaining nodes with FD relaying in cooperative NOMA networks. The literature on NOMA using SWIPT-based full-duplex relay (FDR) is still a challenge at present. In [16], the study analyzed the outage performance of the FD cooperative NOMA network utilizing beamforming and EH. It was demonstrated that SWIPT in cooperative NOMA promotes user collaboration and reduces the effect of self-interference. In [17], the beamforming vector and PS ratio were optimized to maximize the energy efficiency of the FD cooperative NOMA network, where the NU collaborates with the FU. In [18], Expressions for the ergodic capacity and outage probability of the FD cooperative NOMA network with a TS EH protocol at the NU were derived. A study investigated a dedicated EH FD relay in a NOMA system to improve the FU's performance [19]. In [20], the base station and relay used multiple antennas and optimized beamforming to maximize energy efficiency. Expressions for energy efficiency and throughput of an uplink NOMA network with SWIPT were derived [21]. In [22], a mobile edge computing system based on NOMA, aided by unmanned aerial vehicles (UAVs), demonstrated the highest secrecy capacity. In [23], federated learning was utilized to decrease the total energy consumption of NOMA-enabled device communication. In [24], PS-based SWIPT was examined in NOMA, and a union constraint on the error rate was obtained.

The DL between the source and the FU is disregarded in all of the works above, which is sometimes unreasonable. A linear EH model (L-EH) that has a linear connection between the harvested energy and the EH receiver's input energy has been explored in previous research. However, using components with non-linear properties like transistors and diodes limits the efficiency of EH circuits [25]. Because of this non-linearity, the harvested energy saturates when the input energy is above a threshold. In [26], non-linear energy harvesting (NL-EH) is discussed but does not consider the DL performance. A recent study analyzed an NL-EH-enabled FD cooperative NOMA system and reduced its outage probability by selecting an ideal PS value [27]. To lower the energy consumption of EH-enabled IoT devices in a mobile edge computing configuration, the reinforcement learning-based offloading approach was introduced in [28]. A study on reducing energy consumption in wireless sensor networks using a task-based paradigm was discussed in [29]. Energy management strategies for micro-grids and home automation in the IoT were explored in [30], [31]. Relay-assisted cognitive IoT networks utilising PS-SWIPT-based spectrum sharing were examined in [32] for both amplify-and-forward (AF) and decode-and-forward (DF) relaying strategies.

B. MOTIVATIONS AND CONTRIBUTIONS

Communication links are less reliable due to unpredictable and weak energy from fading channels [33]. One potential method is storing energy in batteries or super-capacitors until it is enough to transmit [34]. Super-capacitors cannot hold charge for an extended period, while rechargeable batteries increase the complexity and cost of devices and their form factor. Communication IoT devices with long battery life are needed for industrial applications [35]. Depending solely on the harvested energy is impractical for meeting the performance criteria. For these reasons, using the least amount of battery energy possible to supplement the harvested energy is advisable [26]. In NOMA-based industrial IoT networks, cooperation among devices constantly improves connectivity and spectral efficiency [36].

Using EH-based FD IoT nodes can improve spectral and energy efficiency. However, performance degradation can occur when transmitting at high power levels due to self-loop interference [37]. Therefore, it is fundamental to consider node-level energy efficiency in battery-assisted FD EH communication nodes. Despite its practical significance, the DL between the source and the FU has not yet been addressed on battery-assisted EH relaying in cooperative NOMA. Using the DF relay (and optimum combining) with the DL would increase SNR and give diversity gain. In our analysis, we consider the potential impact of SIC errors in NOMA on IoT applications in the real world. The NOMA protocol instructs the NU first to decode the symbol intended for the FU. Then, they must use SIC to cancel the signal corresponding to the FU from the received signal before decoding their symbol. SIC is perfect if the NU has an ideal estimate of the symbols corresponding to the FU. This leads to the perfect cancellation of the corresponding interference term at the NU. However, when imperfect channel estimates exist, ideal SIC conditions cannot be ensured [38]. This results in residual interference generated at the NU due to imperfect SIC (i-SIC). The perfect SIC is complex in practice due to hardware implementation issues such as error propagation, complexity scaling, and quantization error. These factors can lead to decoding errors and reduce the capability of users during the SIC process.

Understanding the impact of the DL on various parameters such as outage probability, throughput, energy efficiency, EH parameter, and target rate is crucial. Since IoT circuitry has limitations, using NL-EH models in the analysis is vital. Furthermore, it is essential to use supplementary battery energy intelligently while optimally utilizing harvested and EH parameters to ensure prolonged battery life and optimize system performance.

The following are the main contributions of this work:

- In a battery-assisted cooperative NOMA relay network (where the NU serves as an FD DF relay), we analyze the outage and throughput performance of the PS EH protocol While considering the availability of the DL from the source to the FU, NL-EH at the NU and assuming i-SIC at the NU. We take into account two scenarios: (1) no direct link (NDL) between the BS and the FU, (2) direct link (DL) between the BS and the FU. The DL at the FU is evaluated in two scenarios: as an optimal combination to the signal from the NU and as an interfering link to the signal from the NU. It is shown that an optimal combination of the signals from the NU and the source at the FU always results in better performance of the FU. For all scenarios of NDL, interfering direct link (IDL), and maximal ratio combining (MRC) at the FU, closed-form expressions for the outage probability and throughput for the NU and FU are obtained.
- Based on the derived equations, we demonstrate that adding a quantum of battery energy to the harvested energy yields a significant improvement in the FU throughput in MRC. At the same time, the NU performance is essentially unaffected. As the value of i-SIC increases, the outage probability of the NU increases. MRC significantly increases the FU's throughput.
- We derive highly accurate high-SNR expressions for outage probability to determine diversity orders in L-EH and NL-EH cases for DL and NDL scenarios. We demonstrate that NL-EH generates a floor in the outage probability for high transmit power without the DL (diversity gain is 0). When the direct and relayed signals are combined optimally, the performance is improved. In the presence of the DL with MRC, we achieve a diversity gain of one using NL-EH.
- We demonstrate how the power allocation coefficient, the EH parameter, the battery energy, variable node distances, self-loop interference and the saturation threshold impact performance in the NDL and DL situations. There is concavity of throughput with respect to energy harvesting parameter. There is a certain value of the battery energy Q_b that optimises throughput. Thus, there is an operational range $[0, Q_b{}^*]$ where increasing Q_b results in higher throughput. Careful selection of these factors is required to reduce the outage probability and increase throughput. Modifying the distances between the nodes in our system does not impact its performance.
- We have derived an expression for energy efficiency using the derived throughput expressions for the NDL and DL scenarios. Our results show that energy efficiency can be maximized by jointly selecting the optimal battery energy and PS parameter. Regarding the PS protocol, the optimization problem ensures efficient use of the NU's battery energy and has high immunity to self-loop interference.

The paper is organized as follows. Section II describes the system model. The performance of the system is analyzed in Section III. Section IV presents some numerical results. The conclusion is given in Section V.

II. SYSTEM MODEL

A three-node cooperative downlink NOMA architecture consists of a single base station (BS), an NU (D_N), and an FU (D_F) as illustrated in Fig. 1 is considered. The BS communicates directly with the D_N, while the D_F communicates via the relayed link from the D_N and the DL from the BS. Using the decode-and-forward protocol (DF), the data is decoded and sent to D_F, while D_N operates in the FD mode. A single antenna is used on the BS and D_F to simplify the hardware, whereas the D_N has both the transmit and receive antennas as it operates in the FD mode. We will address multiuser and multiple antenna systems in future work. A limited portion of D_N's battery energy is utilised to supplement the harvested energy [26] and create reliable D_N to D_F communication because the harvested

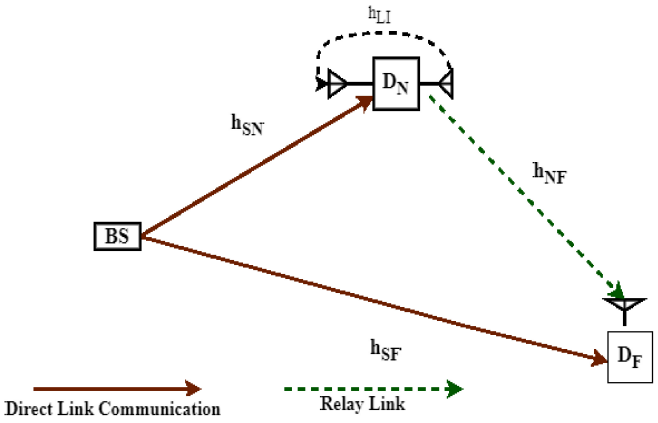

FIGURE 1. Model of the battery-assisted NL-EH downlink FD cooperative NOMA system.

energy is unpredictable and frequently small [39]. Let d_{SN}, d_{SF}, and d_{NF} denote the distances from the BS to D_N, the BS to D_F, and D_N to D_F, respectively. Let h_{ij}, where $i \in (S, N)$ and $j \in (N, F)$, signify the complex fading coefficients corresponding to the links between nodes i and j that are statistically independent and of quasi-static Rayleigh fading type. The complex channel coefficient between nodes i and j is denoted by $h_{ij} \sim \mathcal{CN}(0, 1/\lambda_{ij})$, where $\lambda_{ij} = d_{ij}^{\theta}$ and θ is the path loss exponent, and $\mathcal{CN}(\mu, \sigma^2)$ denotes the complex circular normal distribution with mean μ and variance σ^2.

Self-loop interference (LI) exists from the transmitter to the receiver antennas at D_N while it is in FD mode and is denoted by $h_{LI} \sim \mathcal{CN}(0, g_{LI})$. LI is problematic, but techniques such as antenna cancellation, radio frequency cancellation, signal processing, and others can reduce this LI's strength. However, LI persists in the receiver when decoding the desired signal due to insufficient self-interference cancellation. Alternative tactics have been proposed to address this issue in FD systems. Despite these developments, studies have shown that FD nodes are affected by LI, which is directly related to the transmit power used at the FD relay nodes [40], [41]. Analogue and digital cancellation can provide up to 110 dB of LI cancellation [42]. We assume that LI suppression is of high quality but imperfect in this work. The fact that $\mathbb{E}[|h_{LI}|^2]$ is so little justifies the substitution of g_{LI} for $|h_{LI}|^2$ [43]; note that $\mathbb{E}[\cdot]$ denotes the expectation operator.

The BS obtains the average values of the channel gains through a feedback channel. It is important to note that the energy required to get these average channel gains is significantly less than the energy needed for information transmission (IT) [13], [44]. Under these assumptions, this study aims to evaluate the performance of the PS EH protocol for DF FD NOMA systems. The study examines the system's performance in the DL and the NDL scenarios. The study also analyses the impact of various system parameters, such as the EH parameter, battery energy, power allocation coefficient, node distances, and LI on the throughput and energy efficiency. The research also shows the optimal values of the EH parameters to maximise throughput or minimise battery energy consumption at D_N via thorough simulations.

The system model discussed in this paper has various applications in wireless sensor networks and body area networks. In such networks, neighbouring nodes use their battery energy to relay information to distant nodes [45], [46]. Communication devices in these networks are often battery-powered and have strict requirements on battery lifetimes. Therefore, a node shouldn't drain its battery to relay information. To avoid frequent battery replacement, using EH for relaying is advantageous as it prolongs the battery lifetime of the communication nodes. This paper proposes efficient battery energy utilization and harvesting strategies to achieve this. In addition, sustainable IoT devices can cooperate with other nearby devices for industrial IoT applications in future-generation networks. For such communication devices, a significant battery life is desired [47]. To satisfy the performance requirements, there are other options than depending solely on the harvested energy. Augmenting the harvested energy with as little battery energy as possible is a promising alternative in the future. Device cooperation in NOMA-based industrial IoT networks helps achieve massive connectivity and improved spectrum efficiency.

The paper also derives an expression for energy efficiency using the derived throughput expressions for the NDL and DL scenarios. The results show that energy efficiency can be maximized by jointly selecting the optimal battery energy and PS parameters. Regarding the PS protocol, the optimization problem ensures efficient use of D_N's battery energy and has high immunity to LI. The paper also demonstrates how various parameters such as the power allocation coefficient, the EH parameter, the battery energy, variable node distances, LI and the saturation threshold impact performance in the NDL and DL situations. Overall, this work provides reliable guidance for engineering applications of NOMA and the parameters involved in this work. It indicates the application scenarios corresponding to the parameters to provide clear guidance for the application and development of NOMA.

Let $x_N[m]$ and $x_F[m]$ represent the information symbols intended for D_N and D_F, respectively. Let $P_s = E_s R_s$ denote the transmit power of the BS, where E_s is the symbol energy and R_s is the symbol rate. The BS transmits the superposition of these two symbols represented by $x[m]$, given by

$$x[m] = \sqrt{E_s a_n} x_n[m] + \sqrt{E_s (1 - a_n)} x_f[m] \tag{1}$$

where, for D_N and D_F, the appropriate power allocation coefficients are a_N and $a_F = 1 - a_N$, respectively. We assume that $a_F > a_N$ with $a_N + a_F = 1$. It should be noted that $x_N[m]$ and $x_F[m]$ are normalized unity power signals, i.e., $\mathbb{E}[x_N^2[m]] = \mathbb{E}[x_F^2[m]] = 1$. The received signal (sampled

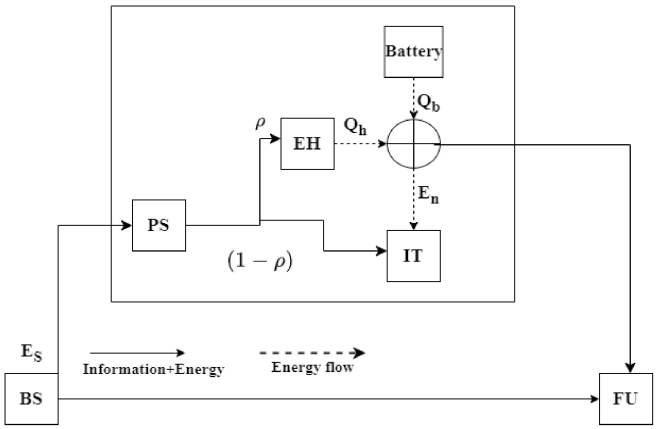

FIGURE 2. Block diagram of the battery-assisted NL-EH downlink FD cooperative NOMA system.

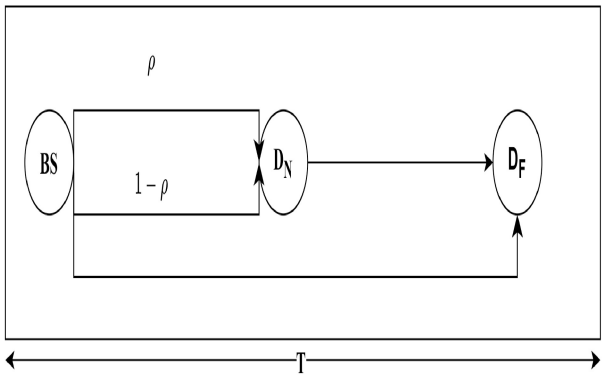

FIGURE 3. Timing diagram for the PS EH protocol transmission system.

matched filter output) at D_N in the m-th time slot is given by

$$y_{D_N}[m] = h_{SN}x[m] + h_{LI}\sqrt{E_n}x_{LI}[m-\tau] + n_{D_N}[m] \quad (2)$$

where $n_{D_N}[m] \sim \mathcal{CN}(0, \sigma^2)$ represents the additive white Gaussian noise (AWGN) at D_N. Let τ be the processing delay at D_N, which is an integer with $\tau \geq 1$, $x_{LI}[m-\tau]$ represent the LI signal, and E_n be the available transmit energy at D_N.

A. ENERGY HARVESTING MODEL

Let us define the PS EH parameter as ρ and the signalling duration as T. In the PS process, a fraction ρ of the signal power received at D_N is reserved for EH, while the remaining $(1-\rho)$ is used for IT, as shown in Fig. 2 and Fig. 3. The TS and PS EH protocols rely on different hardware architectures. Therefore, D_N can use either the TS or PS protocol for EH and IT, but it cannot operate simultaneously in the two EH modes. In the TS scheme, if α represents the TS EH parameter, the αT duration is fixed for EH, meaning that D_N does not transmit during the EH phase. However, in the IT phase, i.e., in the $(1-\alpha)T$ duration, the BS transmits to D_N, and D_N then transmits the decoded symbol to D_F. PS achieves higher throughput but has complex circuitry [14], while TS is more energy-efficient in some cases [15]. We will address both EH protocols in our future work. Compared to the energy needed for IT, the energy required for the activities at D_N (such as threshold activation and information decoding) is essentially insignificant [26]. Since the PS protocol is being used, a component $y^h_{D_N}[m]$ of $y_{D_N}[m]$ may be deduced using the relation

$$y^h_{D_N}[m] = \rho y_{D_N}[m]$$

where the range for the PS parameter ρ is given by $\rho \in [0, 1]$.

This study examines an NL-EH model to highlight the influence of saturation features of the realistic EH circuit [48]. In the literature, two standard models describe NL-EH. The first one, introduced in [25], uses an NL sigmoidal function, while the second is a piecewise NL-EH model [48]. Both models are based on curve-fitting tools, and neither is superior. Therefore, either model can be used to model NL-EH. However, the two-piece-based EH model, used in [48] with similar values for the saturation threshold, is preferred over the sigmoidal function-based model because it allows for a more manageable analysis. In [48], a piece-wise-linear EH model was considered, and the authors studied the effect of sensitivity and saturation threshold characteristics of the energy harvester. NL-EH models are more accurate in describing practical nonlinear circuits. The input energy available for EH per symbol interval taking into account the negligible antenna noise is [44]

$$E_{in} = \rho\Big(|h_{SN}|^2 E_s + E_n g_{LI}\Big), \quad (3)$$

where $(E_n \times g_{LI})$ represents the self-recycled energy arising due to LI at D_N. The amount of energy that is harvested at each symbol interval for NL-EH is represented as [25]

$$Q_h = \begin{cases} \eta E_{in}, & \text{if } E_{in} < E_{sat}, \\ \eta E_{sat}, & \text{if } E_{in} \geq E_{sat}, \end{cases} \quad (4)$$

where $\eta \in [0, 1]$ represents the linear region conversion efficiency of the EH circuit and E_{sat} represents the saturation threshold. Note that L-EH is a particular case when $(E_{sat} \to \infty)$. The quality of service (QoS) is relatively low because of the random nature of the harvested energy. As a result, to improve the QoS, a quantum of battery energy Q_b is added to each symbol. Therefore, the available transmit energy at D_N may be represented as the sum of the harvested energy and the battery energy, i.e., $E_n = Q_h + Q_b$. Using (3), E_n can be written as

$$E_n = \begin{cases} \frac{\eta\rho|h_{SN}|^2 E_s + Q_b}{C_l}, & \text{if } E_{in} < E_{sat}, \\ \eta E_{sat} + Q_b, & \text{if } E_{in} \geq E_{sat}, \end{cases} \quad (5)$$

where $(C_l = 1 - \eta\rho g_{LI})$. Due to high interference cancellation, $g_{LI} \ll 1$ [44], and thus C_l is always positive.

The portion of the received signal at D_N given by (2) utilized for information processing is represented by

$$y^{IP}_{D_N}[m] = \sqrt{1-\rho}\, y_{D_N}[m] + n_{D_N}[m].$$

Since D_F has the high transmit power, D_N first decodes D_F. Next, using the superposed signal, the D_F signal is identified. As a result, the received signal-to-interference-plus-noise ratio (SINR) at D_N to detect D_F's message x_F is

$$\gamma_{D_F \to D_N} = \begin{cases} \frac{|h_{SN}|^2(1-a_N)\gamma_s C_l}{|h_{SN}|^2 a_N \gamma_s C_l + g_{LI}(\eta\rho|h_{SN}|^2\gamma_s+\gamma_b)+\frac{C_l}{1-\rho}}, \\ \text{if } E_{in} < E_{sat}, \\ \frac{|h_{SN}|^2(1-a_N)\gamma_s}{|h_{SN}|^2 a_N \gamma_s + g_{LI}(\eta\gamma_{sat}+\gamma_b)+\frac{1}{1-\rho}}, \\ \text{if } E_{in} \geq E_{sat} \end{cases} \tag{6}$$

where $\gamma_s = E_s/\sigma^2$, $\gamma_b = Q_b/\sigma^2$, and $\gamma_{sat} = E_{sat}/\sigma^2$.

Assuming i-SIC at D_N, the received SINR at D_N used to detect its own message x_N is given by

$$\gamma_{D_N} = \begin{cases} \frac{|h_{SN}|^2 a_N \gamma_s C_l}{\zeta|h_{SN}|^2 a_F \gamma_s + g_{LI}(\eta\rho|h_{SN}|^2\gamma_s+\gamma_b)+\frac{C_l}{1-\rho}}, \\ \text{if } E_{in} < E_{sat}, \\ \frac{|h_{SN}|^2 a_N \gamma_s}{\zeta|h_{SN}|^2 a_F \gamma_s + g_{LI}(\eta\gamma_{sat}+\gamma_b)+\frac{1}{1-\rho}}, \\ \text{if } E_{in} \geq E_{sat}. \end{cases} \tag{7}$$

where the i-SIC factor is represented by ζ $(0 < \zeta < 1)$ and the residual interference caused by i-SIC is represented by $(\zeta|h_{SN}|^2 a_F \gamma_s)$.

The signal received at D_F in the FD mode is written as

$$y_{D_F}[m] = h_{SF}x[m] + h_{NF}\sqrt{E_n}x_F[m-\tau] + n_{D_F}[m] \tag{8}$$

where $n_{D_F[m]} \sim \mathcal{CN}(0, \sigma^2)$ represents the AWGN at D_F. However, for the DL, the observation at D_F is expressed as

$$y_{1,D_F}[m] = h_{SF}x[m] + n_{D_F}[m]. \tag{9}$$

The received SINR at D_F to detect x_F for the DL is

$$\gamma_{1,D_F}^{RI} = \begin{cases} \frac{|h_{SF}|^2 a_F \gamma_s C_l}{|h_{SF}|^2 a_N \gamma_s C_l + \kappa|h_{NF}|^2(\eta\rho|h_{SN}|^2\gamma_s+\gamma_b)+C_l}, \\ \text{if } E_{in} < E_{sat}, \\ \frac{|h_{SF}|^2 a_F \gamma_s}{|h_{SF}|^2 a_N \gamma_s + \kappa|h_{NF}|^2(\eta\gamma_{sat}+\gamma_b)+1}, \\ \text{if } E_{in} \geq E_{sat}, \end{cases} \tag{10}$$

where κ represents the impact levels of the relaying link's *residue interference* (RI). The observation at D_F for the relaying link is written as

$$y_{2,D_F}[m] = h_{NF}\sqrt{E_n}x_F[m-\tau] + n_{D_F}[m].$$

The received SINR at D_F to detect x_F for the relaying link with the impact of the RI from the DL is given by

$$\gamma_{2,D_F}^{RI} = \begin{cases} \frac{|h_{NF}|^2(\eta\rho|h_{SN}|^2\gamma_s+\gamma_b)}{C_l(\kappa|h_{SF}|^2\gamma_s+1)}, & \text{if } E_{in} < E_{sat}, \\ \frac{|h_{NF}|^2(\eta\gamma_{sat}+\gamma_b)}{\kappa|h_{SF}|^2\gamma_s+1}, & \text{if } E_{in} \geq E_{sat}. \end{cases} \tag{11}$$

Firstly, it's important to note that when a symbol is transmitted, the corresponding signal replica from D_N reaches its destination shortly after the replica from the BS. This is due to a processing delay τ, resulting in a temporal separation between the signal replicas from the BS and D_N. To establish a theoretical performance benchmark for practical systems, we assume that these replicas are fully resolvable so they can be appropriately co-phased and merged via MRC. This assumption is based on the ideal operation of rake receivers, which are widely used in wireless systems and follow a theoretical approach known as linear relaying, as introduced in [49]. Most of the analysis and numerical results are presented for the DL with MRC due to its ability to increase SNR and provide diversity gain. The relaying connection from the BS to D_F slightly delays any signals broadcast, much like the DL's relaying link, as seen in [50] and [51]. Put otherwise, there is a temporal difference between the signals from D_N and the BS. To get theoretical findings for real-world NOMA systems [52], we assume that D_N and the BS signals are fully resolvable by D_F. As a result, we offer upper bounds on (10) and (11), the received SINRs at D_F to get x_F for the relaying link and the DL, respectively, as

$$\gamma_{1,D_F} = \begin{cases} \frac{|h_{SF}|^2\gamma_s a_F}{|h_{SF}|^2\gamma_s a_N+1}, & \text{if } E_{in} < E_{sat}, \\ \frac{|h_{SF}|^2\gamma_s a_F}{|h_{SF}|^2\gamma_s a_N+1}, & \text{if } E_{in} \geq E_{sat}, \end{cases} \tag{12}$$

and

$$\gamma_{2,D_F} = \begin{cases} \frac{|h_{NF}|^2(\eta\rho|h_{SN}|^2\gamma_s+\gamma_b)}{C_l}, & \text{if } E_{in} < E_{sat}, \\ |h_{NF}|^2(\eta\gamma_{sat}+\gamma_b), & \text{if } E_{in} \geq E_{sat}. \end{cases} \tag{13}$$

The signals from the relaying link and the DL are mixed using MRC at D_F. As a result, following MRC at D_F, the received SINR is given by

$$\gamma_{D_F}^{MRC} = \begin{cases} \frac{|h_{SF}|^2\gamma_s a_F}{|h_{SF}|^2\gamma_s a_N+1} + \frac{|h_{NF}|^2(\eta\rho|h_{SN}|^2\gamma_s+\gamma_b)}{C_l}, \\ \text{if } E_{in} < E_{sat}, \\ \frac{|h_{SF}|^2\gamma_s a_F}{|h_{SF}|^2\gamma_s a_N+1} + |h_{NF}|^2(\eta\gamma_{sat}+\gamma_b), \\ \text{if } E_{in} \geq E_{sat}. \end{cases} \tag{14}$$

In practical circumstances, D_N will need more time than one symbol period to decode symbols from the BS. Consequently, two symbols will reach D_F from the BS and D_N at any given symbol interval. As a result, the SINR for decoding the symbol X_F at D_F while treating the DL as an interfering link is given by

$$\gamma_{D_F}^{IDL} = \begin{cases} \frac{|h_{NF}|^2(\eta\rho|h_{SN}|^2\gamma_s+\gamma_b)}{C_l(\delta|h_{SF}|^2\gamma_s+1)}, & \text{if } E_{in} < E_{sat}, \\ \frac{|h_{NF}|^2(\eta\gamma_{sat}+\gamma_b)}{\delta|h_{SF}|^2\gamma_s+1}, & \text{if } E_{in} \geq E_{sat}. \end{cases} \tag{15}$$

Here $\delta \in \{0, 1\}$ is used to denote the presence or absence of the DL in the system. Suppose the DL between the BS and D_F is weak due to shadowing and long propagation distance. In that case, it can cause interference to the relayed link from the D_N, so we consider the DL absent or interfering direct link (IDL).

III. PERFORMANCE ANALYSIS

A. OUTAGE PROBABILITY

1) USER RELAYING WITHOUT THE DL

a) Outage Probability of D_N: According to the NOMA protocol, D_N's outage probability is stated in terms of its complementing events as

$$P_{D_N}^{FD} = 1 - P_r\Big(\gamma_{D_F \to D_N} > \gamma_{th_F}^{FD}, \gamma_{D_N} > \gamma_{th_N}^{FD}\Big), \tag{16}$$

where R_N is the target rate to detect x_N at D_N, $\gamma_{th_N}^{FD} = 2^{2R_N}-1$, R_F is the target rate for detecting x_F at D_N, and $\gamma_{th_F}^{FD} = 2^{R_F} - 1$. Using the battery-assisted SWIPT PSR protocol, the outage probability expression in (16) can be written as

$$P_{D_N}^{FD} = 1 - P_r\Big(E_{in} < E_{sat}, \gamma_{D_F\to D_N} > \gamma_{th_F}^{FD}, \gamma_{D_N} > \gamma_{th_N}^{FD}\Big) - P_r\Big(E_{in} \geq E_{sat}, \gamma_{D_F\to D_N} > \gamma_{th_F}^{FD}, \gamma_{D_N} > \gamma_{th_N}^{FD}\Big). \quad (17)$$

Let us denote the channel gains as $|h_{SN}|^2 = X$, $|h_{NF}|^2 = Y$, and $|h_{SF}|^2 = Z$. We can write (17) as

$$P_{D_N}^{FD} = 1 - \underbrace{P_r(\max(\beta_1, \theta_1) < X < \phi_1)}_{I_1} - \underbrace{P_r(X > \max(\phi_2, \beta_2, \theta_2))}_{I_2} \quad (18)$$

$$\phi_1 = \frac{1}{E_s}\left(\frac{C_l E_{sat}}{\rho} - Q_b g_{LI}\right),$$

$$\beta_1 = \frac{\gamma_{th_F}^{FD}\left(g_{LI}\gamma_b + \frac{C_l}{1-\rho}\right)}{\gamma_s\left(a_F C_l - \gamma_{th_F}^{FD} a_N C_l - \gamma_{th_F}^{FD} g_{LI}\eta\rho\right)},$$

$$\theta_1 = \frac{\gamma_{th_N}^{FD}\left(g_{LI}\gamma_b + \frac{C_l}{1-\rho}\right)}{\gamma_s\left(a_N C_l - \gamma_{th_N}^{FD}\zeta a_F - \gamma_{th_N}^{FD} g_{LI}\eta\rho\right)},$$

$$\phi_2 = \frac{1}{E_s}\left(\frac{E_{sat}}{\rho} - (\eta E_{sat} + Q_b) g_{LI}\right),$$

$$\beta_2 = \frac{\gamma_{th_F}^{FD}\left(g_{LI}(\eta\gamma_{sat} + \gamma_b) + \frac{1}{1-\rho}\right)}{\gamma_s\left(a_F - \gamma_{th_F}^{FD} a_N\right)},$$

$$\theta_2 = \frac{\gamma_{th_N}^{FD}\left(g_{LI}(\eta\gamma_{sat} + \gamma_b) + \frac{1}{1-\rho}\right)}{\gamma_s\left(a_N - \gamma_{th_N}^{FD}\zeta a_F\right)}.$$

Lemma 1: The outage probability of D_N using NL-EH augmented with battery energy at D_N is given by the closed-form expression

$$P_{D_N}^{FD} = 1 - \left(e^{-\lambda_{SN}\max(\beta_1,\theta_1)} - e^{-\lambda_{SN}\phi_1}\right) - \left(e^{-\lambda_{SN}\max(\phi_2,\beta_2,\theta_2)}\right). \quad (19)$$

Proof: By definition, the complementary events at D_N are denoted by I_1 and I_2 and calculated as

$$I_1 = \int_{\max(\beta_1,\theta_1)}^{\phi_1} f_{|h_{SN}|^2}(x)dx = \left(e^{-\lambda_{SN}\max(\beta_1,\theta_1)} - e^{-\lambda_{SN}\phi_1}\right),$$

$$I_2 = \int_{\max(\beta_2,\theta_2,\phi_2)}^{\infty} f_{|h_{SN}|^2}(x)dx = \left(e^{-\lambda_{SN}\max(\phi_2,\beta_2,\theta_2)}\right).$$

Substituting I_1 and I_2 in (18), (19) is obtained. ■

Remark 1: The performance of L-EH can be easily obtained by setting E_{sat} or $\gamma_{sat} \to \infty$ in (19). The outage probability of D_N, in this case, is given as

$$P_{D_N}^{FD,L} \simeq 1 - \left(e^{-\lambda_{SN}max(\beta_1,\theta_1)} - e^{-\lambda_{SN}\phi_1}\right). \quad (20)$$

Remark 2: Using simple mathematical simplifications, first-order linear approximations of the exponential components, and ignoring the higher order terms in $1/\gamma_s$, the outage probability of D_N for high SNR approximation ($\gamma_s \to \infty$) is obtained and is given by

$$P_{D_N}^{FD,\infty} \simeq \lambda_{SN}\max(\beta_1, \theta_1) - \lambda_{SN}\phi_1 + \lambda_{SN}\max(\beta_2, \theta_2, \phi_2). \quad (21)$$

b) Outage Probability of D_F: The D_F outage occurrences may be characterised as follows. One limitation is that D_N cannot identify x_F. The second point is that D_F cannot determine its message x_F under the same circumstances that D_N can successfully detect x_F. The outage probability of D_F is obtained as

$$P_{D_F,nodir}^{FD} = 1 - P_r\Big(\gamma_{D_F\to D_N} > \gamma_{th_F}^{FD}, \gamma_{2,D_F} > \gamma_{th_F}^{FD}\Big). \quad (22)$$

Using the battery-assisted SWIPT PSR protocol, the outage probability expression in (22) can be written as

$$P_{D_F,nodir}^{FD} = 1 - P_r\Big(E_{in} < E_{sat}, \gamma_{D_F\to D_N} > \gamma_{th_F}^{FD}, \gamma_{2,D_F} > \gamma_{th_F}^{FD}\Big) - P_r\Big(E_{in} \geq E_{sat}, \gamma_{D_F\to D_N} > \gamma_{th_F}^{FD}, \gamma_{2,D_F} > \gamma_{th_F}^{FD}\Big). \quad (23)$$

We can express (23) as

$$P_{D_F,nodir}^{FD} = 1 - \underbrace{P_r\left(\beta_1 < X < \phi_1, Y > \frac{C_l\gamma_{th_F}^{FD}}{\eta\rho X\gamma_s + \gamma_b}\right)}_{I_1} - \underbrace{P_r\left(X > \max(\phi_2, \beta_2), Y > \frac{\gamma_{th_F}^{FD}}{\eta\gamma_{sat} + \gamma_b}\right)}_{I_2}. \quad (24)$$

Lemma 2: The outage probability of D_F using NL-EH augmented with battery energy D_N is provided by the closed form expression given in (25)

$$P_{D_F,nodir}^{FD} \simeq 1 - \left\{\left(e^{-\lambda_{SN}\beta_1} - e^{-\lambda_{SN}\phi_1}\right) - \frac{\lambda_{NF}\lambda_{SN}C_l\gamma_{th_F}^{FD}}{\eta\rho\gamma_s} \times\left[e^{\mu_1\lambda_{SN}}\begin{pmatrix} E_i(-(\mu_1+\phi_1)\lambda_{SN}) \\ -E_i(-(\mu_1+\beta_1)\lambda_{SN})\end{pmatrix}\right]\right\} - \left(e^{-\lambda_{SN}\max(\phi_2,\beta_2) - \frac{\lambda_{NF}\gamma_{th_F}^{FD}}{\eta\gamma_{sat}+\gamma_b}}\right) \quad (25)$$

where

$$\mu_1 = \frac{\gamma_b + \lambda_{NF}C_l\gamma_{th_F}^{FD}}{\eta\rho\gamma_s}.$$

and $E_i(\cdot)$ is given by *[54, Eq. (8.211.1)]*.

Proof: See Appendix A. ■

Remark 3: The performance of the L-EH model may be easily attained by setting E_{sat} or $\gamma_{sat} \to \infty$ in (25). The outage probability of D_F, in this case, is given as

$$P_{D_F,nodir}^{FD,L} \simeq 1 - \left\{ \left(e^{-\lambda_{SN}\beta_1} - e^{-\lambda_{SN}\phi_1}\right) - \frac{\lambda_{NF}\lambda_{SN}C_l\gamma_{th_F}^{FD}}{\eta\rho\gamma_s} \times \left[e^{\mu_1\lambda_{SN}} \begin{pmatrix} E_i(-(\mu_1+\phi_1)\lambda_{SN}) \\ -E_i(-(\mu_1+\beta_1)\lambda_{SN}) \end{pmatrix} \right] \right\}. \quad (26)$$

Remark 4: An outage floor in D_F performance is caused by γ_{sat} at high transmit powers. This outage floor may be determined with an asymptotic equation of $P_{D_F,nodir}^{FD}$. Using simple mathematical simplifications, first-order linear approximations of the exponential components, and ignoring the higher order terms in $1/\gamma_s$, and putting $e^u E_1(u)=1/(1+u)$ [53, 5.1.19] at high values of γ_s, the outage probability of D_F for the high SNR approximation ($\gamma_s \to \infty$) is obtained and is given by (27).

$$P_{D_F,nodir}^{FD,\infty} \simeq 1 + \lambda_{SN}\beta_1 - \lambda_{SN}\phi_1 - \frac{\lambda_{NF}\lambda_{SN}C_l\gamma_{th_F}^{FD}}{\eta\rho\gamma_s} \begin{bmatrix} \frac{1}{1+(\mu_1+\phi_1)\lambda_{SN}} \\ -\frac{1}{1+(\mu_1+\beta_1)\lambda_{SN}} \end{bmatrix} - (1-\lambda_{SN}\max(\phi_2,\beta_2)) \left(\frac{\eta\gamma_{sat}+\gamma_b}{\eta\gamma_{sat}+\gamma_b+\lambda_{NF}\gamma_{th_F}^{FD}} \right). \quad (27)$$

2) USER RELAYING WITH DL

a) Outage Probability of D_F: There are two potential outage scenarios for FD NOMA with D_F. The first event happens when x_F can be detected at D_N, but the received SINR after MRC at D_F in one slot is lower than the desired SNR. The second event occurs when neither D_N nor D_F can identify x_F. The outage probability of D_F with the DL is given as

$$P_{D_F,dir}^{FD,RI} = P_r\left(\gamma_{1,D_F}^{RI} + \gamma_{2,D_F}^{RI} < \gamma_{th_F}^{FD}, \gamma_{D_F\to D_N} > \gamma_{th_F}^{FD}\right) + P_r\left(\gamma_{D_F\to D_N} < \gamma_{th_F}^{FD}, \gamma_{1,D_F}^{RI} < \gamma_{th_F}^{FD}\right). \quad (28)$$

Furthermore, the outage probability of D_F using the upper bounds of the received SINRs are given by

$$P_{D_F,dir}^{FD} = P_r\left(\gamma_{D_F}^{MRC} < \gamma_{th_F}^{FD}, \gamma_{D_F\to D_N} > \gamma_{th_F}^{FD}\right) + P_r\left(\gamma_{D_F\to D_N} < \gamma_{th_F}^{FD}, \gamma_{1,D_F} < \gamma_{th_F}^{FD}\right). \quad (29)$$

Using the battery-assisted SWIPT PSR protocol, the outage probability expression in (29) can be written as

$$\begin{aligned} P_{D_F,dir}^{FD} &= P_r\left(\gamma_{D_F\to D_N} < \gamma_{th_F}^{FD}, \gamma_{1,D_F} < \gamma_{th_F}^{FD}\right) \\ &+ P_r\left(E_{in} < E_{sat}, \gamma_{D_F\to D_N} > \gamma_{th_F}^{FD}, \gamma_{D_F}^{MRC} < \gamma_{th_F}^{FD}\right) \\ &+ P_r\left(E_{in} \geq E_{sat}, \gamma_{D_F\to D_N} > \gamma_{th_F}^{FD}, \gamma_{D_F}^{MRC} < \gamma_{th_F}^{FD}\right). \quad (30) \end{aligned}$$

We can express (30) as

$$P_{D_F,dir}^{FD} = \underbrace{P_r(X<\beta_1, Z<L_1)}_{I_1} + P_r\underbrace{(\beta_1 < X < \phi_1, Y < A_1, Z < L_1)}_{I_2} + \underbrace{P_r(X > max(\phi_2,\beta_2), Y < A_2, Z < L_1)}_{I_3}, \quad (31)$$

where

$$L_1 = \frac{\gamma_{th_F}^{FD}}{\gamma_s\left(a_F - \gamma_{th_F}^{FD}a_N\right)},$$
$$A_1 = \frac{\gamma_{th_F}^{FD}C_l(Z\gamma_s a_N C_l + C_l) - Z\gamma_s a_F C_l^2}{(\eta\rho X\gamma_s + \gamma_b)(Z\gamma_s a_N C_l + C_l)}, \quad \text{and}$$
$$A_2 = \frac{\gamma_{th_F}(Z\gamma_s a_N + 1) - Z\gamma_s a_F}{(\eta\gamma_{sat} + \gamma_b)(Z\gamma_s a_N + 1)}.$$

I_1 (in (31)) is given by

$$I_1 = \left(1 - e^{-\lambda_{SN}\beta_1}\right)\left(1 - e^{-\lambda_{SF}L_1}\right), \quad (32)$$

I_2 (in (31)) is given by (33), and I_3 (in (31)) is given by (34).

$$\begin{aligned} I_2 \simeq\ & e^{-\lambda_{SN}\beta_1}\left(1 - e^{-\lambda_{SF}L_1}\right) - D_1\left(\frac{\gamma_s a_N}{\lambda_{SF}}\left(1 - e^{-\lambda_{SF}L_1}\right)\right. \\ & - D_2\left[e^{\lambda_{SF}D_3}\begin{Bmatrix} E_i(-\lambda_{SF}L_1 - \lambda_{SF}D_3) \\ -E_i(-\lambda_{SF}D_3) \end{Bmatrix}\right] \\ & \left. + \left\{e^{\lambda_{SF}D_3}\begin{pmatrix} E_i(-\lambda_{SF}L_1 - \lambda_{SF}D_3) \\ -E_i(\lambda_{SF}D_3) \end{pmatrix}\right\}\right) \\ & - e^{-\lambda_{SN}\phi_1}\left(1 - e^{-\lambda_{SF}L_1}\right) + D_4\left(\frac{\gamma_s a_N}{\lambda_{SF}}\right. \\ & \times\left(1 - e^{-\lambda_{SF}L_1}\right) - D_5 \\ & \times\left[e^{\lambda_{SF}D_6}\begin{Bmatrix} E_i(-\lambda_{SF}L_1 - \lambda_{SF}D_6) \\ -E_i(-\lambda_{SF}D_6) \end{Bmatrix}\right] \\ & \left. + \left\{e^{\lambda_{SF}D_6}\begin{pmatrix} E_i(-\lambda_{SF}L_1 - \lambda_{SF}D_6) \\ -E_i(\lambda_{SF}D_6) \end{pmatrix}\right\}\right). \quad (33) \end{aligned}$$

Note that

$$D_1 = \frac{\lambda_{SF}e^{-\lambda_{SN}\beta_1}\left(\beta_1 + \frac{\gamma_b}{\eta\rho\gamma_s}\right)\eta\rho}{P_1 + \lambda_{NF}\gamma_{th_F}^{FD}C_l a_N - \lambda_{NF}a_F C_l},$$
$$D_2 = \frac{a_N C_l\left(\eta\rho\gamma_s\beta_1 + \gamma_b + \lambda_{NF}\gamma_{th_F}^{FD}C_l\right)}{P_1 + \gamma_b a_N + \lambda_{NF}\gamma_{th_F}^{FD}C_l a_N - \lambda_{NF}a_F C_l},$$
$$D_3 = \frac{a_N}{\gamma_s}D_2,$$
$$P_1 = (\eta\rho\gamma_s\beta_1 a_N + \gamma_b a_N).$$

Similarly, D_4, D_5, and D_6 are obtained by replacing β_1 with ϕ_1 in D_1, D_2, and D_3, respectively.

$$I_3 \simeq e^{-\lambda_{SN}max(\phi_2,\beta_2)}\left[\left(1 - e^{-\lambda_{SF}L_1}\right) - \frac{D_7}{\lambda_{SF}}\right.$$

$$\times\left(1-e^{-\lambda_{SF}L_1}\right)+\frac{D_7D_8}{\gamma_s}$$
$$\times\left\{e^{\frac{\lambda_{SF}D_8}{\gamma_s}}\begin{pmatrix}E_i\left(-\lambda_{SF}L_1-\frac{\lambda_{SF}D_8}{\gamma_s}\right)\\-E_i\left(\frac{-\lambda_{SF}D_8}{\gamma_s}\right)\end{pmatrix}\right\}$$
$$-\frac{D_9}{\gamma_s}\left\{e^{\frac{\lambda_{SF}D_8}{\gamma_s}}\begin{pmatrix}E_i\left(-\lambda_{SF}L_1-\frac{\lambda_{SF}D_8}{\gamma_s}\right)\\-E_i\left(\frac{-\lambda_{SF}D_8}{\gamma_s}\right)\end{pmatrix}\right\}\Bigg]. \quad (34)$$

Note further that

$$D_7=\frac{\lambda_{SF}a_N(\eta\gamma_{sat}+\gamma_b)}{P_2+a_N\gamma_b+\lambda_{NF}\gamma_{th_F}^{FD}a_N-\lambda_{NF}+\lambda_{NF}a_N},$$
$$D_8=\frac{\eta\gamma_{sat}+\gamma_b+\lambda_{NF}\gamma_{th_F}^{FD}}{P_2+a_N\gamma_b+\lambda_{NF}\gamma_{th_F}^{FD}a_N-\lambda_{NF}+\lambda_{NF}a_N},$$
$$D_9=\frac{D_7}{a_N},$$
$$P_2=(\eta\gamma_{sat}a_N).$$

Substituting the values of I_1, I_2, and I_3 in (31), a closed-form expression of the outage probability of D_F with the DL is obtained.

The derivations of the expressions for I_1, I_2, and I_3 are given in Appendix B.

Remark 5: The performance of the L-EH model may be easily attained by setting E_{sat} or $\gamma_{sat}\to\infty$ in I_3 given by (34).

Remark 6: Using simple mathematical simplifications, first-order linear approximations of the exponential components, and ignoring the higher-order terms in $1/\gamma_s$, and putting $e^uE_1(u)=1/(1+u)$ [53, 5.1.19] at high values of γ_s, the high SNR approximations ($\gamma_s\to\infty$) of I_2 and I_3 in (33) and (34), respectively, are obtained and are given by (35) and (36), respectively.

$$I_2^{\infty}\simeq(\lambda_{SF}L_1)-D_1\Bigg\{\gamma_sa_NL_1+D_2\begin{pmatrix}\frac{1}{1+\lambda_{SF}(L_1+D_3)}\\-\frac{1}{1+\lambda_{SF}D_3}\end{pmatrix}$$
$$-\left(\frac{1}{1+\lambda_{SF}(L_1+D_3)}-\frac{1}{1+\lambda_{SF}D_3}\right)\Bigg\}$$
$$-\Bigg[(\lambda_{SF}L_1)-D_4\Bigg\{\gamma_sa_NL_1+D_5\begin{pmatrix}\frac{1}{1+\lambda_{SF}(L_1+D_6)}\\-\frac{1}{1+\lambda_{SF}D_6}\end{pmatrix}$$
$$-\left(\frac{1}{1+\lambda_{SF}(L_1+D_6)}-\frac{1}{1+\lambda_{SF}D_6}\right)\Bigg\}\Bigg]. \quad (35)$$

$$I_3^{\infty}\simeq(\lambda_{SF}L_1)-D_7L_1-\frac{D_7D_8}{\gamma_s}\begin{pmatrix}\frac{1}{1+\lambda_{SF}\left(L_1+\frac{D_8}{\gamma_s}\right)}\\-\frac{1}{1+\lambda_{SF}\frac{D_8}{\gamma_s}}\end{pmatrix}$$
$$+\frac{D_9}{\gamma_s}\begin{pmatrix}\frac{1}{1+\lambda_{SF}\frac{D_8}{\gamma_s}}\\-\frac{1}{1+\lambda_{SF}\frac{D_8}{\gamma_s}}\end{pmatrix}. \quad (36)$$

Remark 7: From $P_{D_N}^{FD}$, $P_{D_F,nodir}^{FD}$ and $P_{D_F,dir}^{FD}$, as the value of ζ increases, the outage probability of D_N becomes more extensive due to the residual interference generated by i-SIC at D_N. However, the outage probability of D_F is insensitive to ζ since SIC is not required to detect symbol x_F at D_N and D_F.

To illustrate the effect of SIC error on the outage probability performance of both D_N and D_F, we have shown the results in Fig. 6. It is clear from Fig. 6 that the SIC error does not affect the D_F outage performance. Meanwhile, the SIC error limits D_N performance. Hence, the SIC error's effect is insignificant on D_F's performance. Therefore, we have considered $\zeta=0$, i.e., the case of perfect SIC in the remaining figures.

b) Outage Probability of D_F With IDL: Suppose the DL between the BS and D_F is weak due to shadowing and long propagation distance. In that case, it can cause interference to the relayed link from the D_N, so we consider the DL absent or IDL. The outage probability of D_F with the IDL is given as

$$P_{D_F,dir}^{IDL}$$
$$=1-P_r\left(E_{in}<E_{sat},\gamma_{D_F\to D_N}>\gamma_{th_F}^{FD},\gamma_{D_F}^{IDL}>\gamma_{th_F}^{FD}\right)$$
$$-P_r\left(E_{in}\geq E_{sat},\gamma_{D_F\to D_N}>\gamma_{th_F}^{FD},\gamma_{D_F}^{IDL}>\gamma_{th_F}^{FD}\right). \quad (37)$$

We can express (37) as

$$P_{D_F,IDL}^{FD}=1$$
$$\underbrace{-P_r\left(\beta_1<X<\phi_1,|h_{NF}|^2>\frac{C_l\gamma_{th_F}^{FD}(\delta Z\gamma_s+1)}{\eta\rho X\gamma_s+\gamma_b}\right)}_{\hat{I}_1}$$
$$\underbrace{-P_r\left(X>\max(\phi_2,\beta_2),Y>\frac{\gamma_{th_F}^{FD}(\delta Z\gamma_s)}{\eta\gamma_{sat}+\gamma_b}\right)}_{\hat{I}_2}. \quad (38)$$

In (38), $\hat{I}_1$ and $\hat{I}_2$ are given by (39) and (40), respectively. In (39),

$$P_1=\frac{e^{-\lambda_{SN}\beta_1}-e^{-\lambda_{SN}\phi_1}}{\lambda_{SN}},$$
$$P_2=E_i(-\phi_1\lambda_{SN})-E_i(\beta_1\lambda_{SN}),$$
$$P_3=\frac{\lambda_{NF}\gamma_{th_F}^{FD}C_l}{\eta\rho\gamma_s+\lambda_{NF}\gamma_b},$$
$$P_4=\frac{{\beta_1}^{-n}(\beta_1\lambda_{SN})^n\Gamma(1-n,\beta_1\lambda_{SN})}{\lambda_{SN}},$$
$$-\frac{{\phi_1}^{-n}(\phi_1\lambda_{SN})^n\Gamma(1-n,\phi_1\lambda_{SN})}{\lambda_{SN}}.$$

In (40),

$$P_5=\frac{\gamma_{th_F}^{FD}}{\eta\gamma_{sat}+\gamma_b}.$$

Here,where $\Gamma(n,x)$ represents the upper incomplete gamma function.

$$\hat{I}_1\simeq\lambda_{SN}P_1-\lambda_{SN}\lambda_{SF}P_2\begin{pmatrix}P_3\delta\gamma_s\left(\frac{1}{\lambda_{SF}}\right)^2\\+P_3\frac{1}{\lambda_{SF}}\end{pmatrix}$$

TABLE 1. Diversity order for L-EH/NL-EH FD NOMA systems.

L-EH/NL-EH NOMA diversity order			
(L/NL)-EH	D_N/D_F	NDL/DL	Diversity
L-EH	D_N/D_F	NDL	1/1
L-EH	D_N/D_F	DL	1/2
NL-EH	D_N/D_F	NDL	1/0
NL-EH	D_N/D_F	DL	1/1

$$+\lambda_{SN}\lambda_{SF}\sum_{n=2}^{\infty}\frac{-1^n}{n!}P_4P_3\binom{n}{k}(\delta\gamma_s)^k \times k!(\lambda_{SF})^{(-k-1)}. \quad (39)$$

$$\hat{I_2} \simeq \lambda_{SN}\lambda_{SF}\frac{e^{-\lambda_{SN}max(\phi_2\beta_2)}}{\lambda_{SN}}\left(\frac{1}{\lambda_{SF}} - P_5\delta\gamma_s \times\left(\frac{1}{\lambda_{SF}}\right)^2 - P_5\frac{1}{\lambda_{SF}} + \sum_{n=2}^{\infty}\frac{-1^n}{n!}P_5^n\binom{n}{k} \times(\delta\gamma_s)^k k!(\lambda_{SF})^{-k-1}\right). \quad (40)$$

Lemma 3: The diversity order (D) is given by

$$D = -\lim_{\gamma_s\to\infty}\frac{\log\left(P_D^{\infty}(\gamma_s)\right)}{\log(\gamma_s)} \quad (41)$$

The diversity order is computed using the high SNR approximations obtained above in (41) and is given in the following table. The values mentioned in the table have been confirmed by simulation results. The DL is crucial to mitigate diversity loss caused by NL-EH.

B. THROUGHPUT ANALYSIS

The throughput of D_N is given as

$$R_{D_N}^{FD} = \left(1 - P_{D_N}^{FD}\right)R_N \quad (42)$$

and for D_F without the DL and with the DL are given, respectively, as

$$R_{D_F,nodir}^{FD} = \left(1 - P_{D_F,nodir}^{FD}\right)R_F \quad (43)$$

$$R_{D_F,dir}^{FD} = \left(1 - P_{D_F,dir}^{FD}\right)R_F. \quad (44)$$

C. ENERGY EFFICIENCY

Energy efficiency is an essential aspect of modern communication systems that involve many connected IoT devices and have limited energy resources. It is the ratio of the sum throughput to the total energy consumption. The metric guarantees these systems' best possible performance and long-term sustainability [55], [56]. The mathematical expression of energy efficiency for the proposed system using the throughput expressions derived for nodes D_N and D_F is expressed as

$$\eta_{\phi}^{FD} = \frac{\text{Total data rate (sum throughput)}}{\text{Total energy consumption}} = \frac{\mathcal{T}_{\phi}^{FD}}{Es + Q_b} \quad (45)$$

where $\mathcal{T}_{\phi}^{FD} = R_{D_N}^{FD} + R_{D_F,\phi}^{FD}$ and $\phi \in (dir, nodir)$.

It is essential to note that D_N first collects the energy from the BS and uses it to send information symbols to D_F. However, the energy harvested may sometimes need to be more, depending on the value of the PS parameter. D_N to D_F information exchange becomes impossible in such cases, and the supplementary battery energy is used to assist D_N to D_F transmission. However, the harvested energy is generally sufficient for high-source transmit powers, and the additional battery energy only increases the LI levels. This can lead to decoding issues for the D_F symbol, decreasing the throughput of D_N and D_F. Using the high transmit power of the BS can degrade energy efficiency. This is because when Q_b is very high, the LI becomes large, which makes it difficult for D_N to decode D_F symbols. As a result, D_F and D_N throughput decrease. Transmitting with high Q_b at D_N can further degrade energy efficiency. Therefore, choosing ρ and Q_b to maximize energy efficiency is crucial. Let $Q_{b,max}$ and $Q_{b,min}$ be the maximum and minimum values of the battery energy that can be drawn. With this in mind, the optimization problem can be formulated as follows:

$$\begin{aligned}\left(Q_b^*, \rho^*\right) = arg\max_{(Q_b,\rho)} \quad & \eta_{\phi}^{FD} \\ \text{s.t.} \quad & 0 < \rho < 1 \\ & Q_{b,min} < Q_b < Q_{b,max}\end{aligned} \quad (46)$$

In the given context, ρ^* represents the optimal parameter for the PS EH protocol. Since the expressions for D_N and D_F outage probabilities are pretty complex, arriving at a closed-form expression for $(Q_b^*, \rho^*))$ is impossible. However, we can determine the optimal point (Q_b^*, ρ^*) through a standard numerical search. ρ and Q_b that maximize throughput also maximize the energy efficiency. To solve the optimization problem (46), we must find a jointly optimal solution for variables ρ and Q_b. However, their coupling makes solving this analytically using standard optimization techniques exceptionally challenging. To overcome this difficulty, we use a 2-D search method to find the optimal solution $(Q_b^*, \rho^*))$. This search method is used exhaustively across the Q_b and ρ range. It's worth mentioning that this 2-D search method is the most commonly used approach to determine the optimal point in a complex but low-dimensional optimization problem. The accuracy of this optimal point depends on the choice of the step size.

In some applications, achieving a specific throughput for D_N may be necessary. It is possible to attain the desired throughput by selecting appropriate ρ and Q_b. However, it is essential to choose these parameters to minimize battery energy consumption while maintaining the required throughput for D_N. To achieve this goal, it is crucial to optimize the symbol rate. We will discuss this topic in future work.

IV. NUMERICAL RESULTS AND DISCUSSIONS

In this section, we provide simulation results to evaluate further the performance of the considered model in a battery-assisted NL-EH model and compare them with the analytical

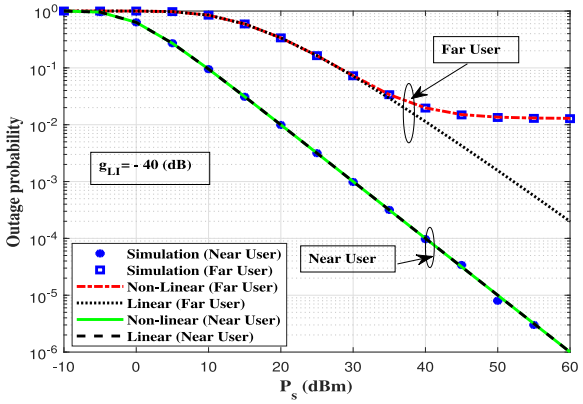

FIGURE 4. Outage probability of D_N and D_F versus the source transmit power without the DL.

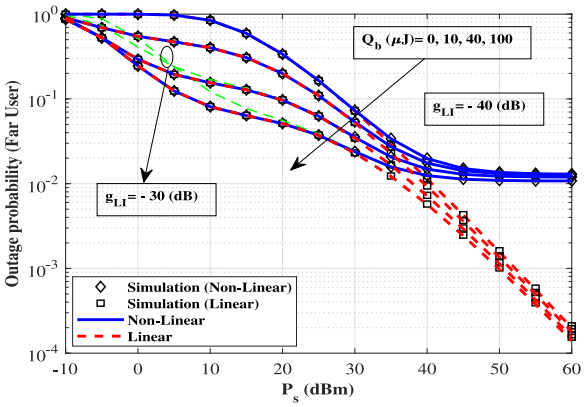

FIGURE 5. Outage probability of D_F versus the source transmit power without the DL.

expressions derived to validate our analysis. The following values are assumed for the parameters unless otherwise specified: the distances between the nodes are specified as $d_{SF} = 16$ units, $d_{SN} = 10$ units, and $d_{NF} = 6$ units; $R_N = 2$, $R_F = 2$; $\rho = 0.7$, $\eta = 0.5$; $\sigma^2 = -50$ dBm; path loss exponent $\theta = 3$ [19], [57], [58]; $a_N = 0.1$, $a_F = 0.9$; saturation threshold $P_{sat} = E_{sat}R_s = 9.2$ μW [48].

The outage probability of the two users versus the source transmit power P_s for the PSR protocol without the DL is plotted in Fig. 4 with $\mathbb{E}[|h_{LI}|^2] = g_{LI} = -40$ dB. Both L-EH and NL-EH performance for the two users are compared. The simulation results verify the accuracy of the obtained analytical expressions. Both the users show a considerable improvement in their outage probability with increasing P_s at low transmit powers. Using the perfect SIC at D_N, D_N performs almost identically in linear and non-linear cases. Nevertheless, when NL-EH is used at D_N, the outage probability of D_F saturates with higher values of P_s (the floor is caused by the γ_{sat} *(saturation threshold)*, which limits the transmit power of D_N). Thus, D_F performs better in L-EH at higher transmit powers.

Let $\mathbb{E}[|h_{LI}|^2] = g_{LI} = -40$ dB. The outage probability of D_F versus the source transmit power P_s for PSR protocol with the NDL is plotted in Fig. 5 for different Q_b values.

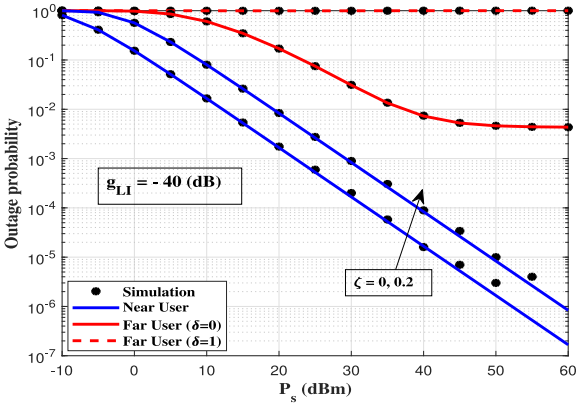

FIGURE 6. Outage probability of D_N and D_F versus the source transmit power with IDL and imperfect SIC.

The simulation results confirm the correctness of the derived analytical expressions. Adding a small amount of battery energy Q_b to the harvested energy greatly improves the outage performance (compared to the case where $Q_b = 0$). Increasing Q_b for both linear and non-linear energy harvesting models results in a noticeable reduction in D_F outage probability for low transmit powers, while the benefit at larger P_s is minimal. The performance of L-EH at high transmit powers is much better than that of NL-EH since the transmit power at D_N in NL-EH is restricted by γ_{sat}. The impact of LI *(self-loop interference)* is negligible for low transmit powers and lower values of Q_b. However, the self-recycled energy $E_n \times g_{LI}$ rises as Q_b does. Thus, it can be shown that when $g_{LI} = -40$ (dB), the outage probability is smaller than in the situation where $g_{LI} = -30$ (dB) when $Q_b = 40(\mu J)$. However, the harvested energy is more important at higher transmit power values. At high transmit powers, the NL-EH in the outage floor results in a diversity loss to D_F.

Let $\mathbb{E}[|h_{LI}|^2] = -40$ dB. Fig. 6 shows the outage probability that D_N and D_F experienced in the NDL and interfering direct link (IDL) cases versus the source transmit power for various values of ζ (i.e., the i-SIC factor). The residual interference generated by i-SIC at D_N causes the outage probability of D_N to increase as ζ increases. However, the outage probability of D_F is insensitive to ζ since SIC is not necessary to identify the symbol x_F at D_F. The results make it abundantly evident that the impact of SIC errors is negligible for the outage probability of D_F. Thus, in the subsequent results, we have considered $\zeta = 0$, or the situation of perfect SIC. It is observed that the interference caused by the DL from the BS to D_F causes the outage probability of D_F to increase significantly for the IDL case compared to the NDL case and using the DL with MRC. Therefore, we have considered the DL with MRC in all the results.

Fig. 7 shows the relationship between the outage probability of D_N and D_F versus a_N for various Q_b and ρ values as well as various R_F and R_N combinations. The simulation

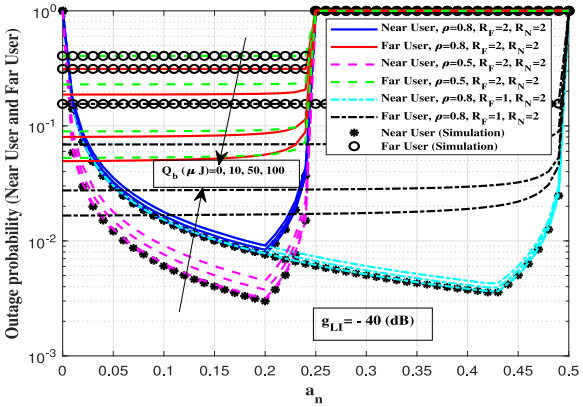

FIGURE 7. Outage probability of (D_N and D_F) versus a_N without the DL.

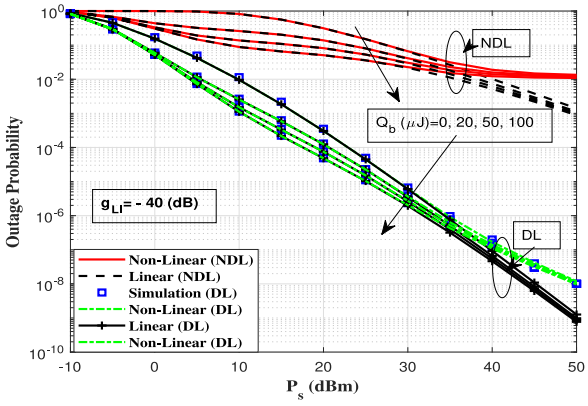

FIGURE 8. Outage probability of D_F versus the source transmit power without the DL and with the DL using MRC.

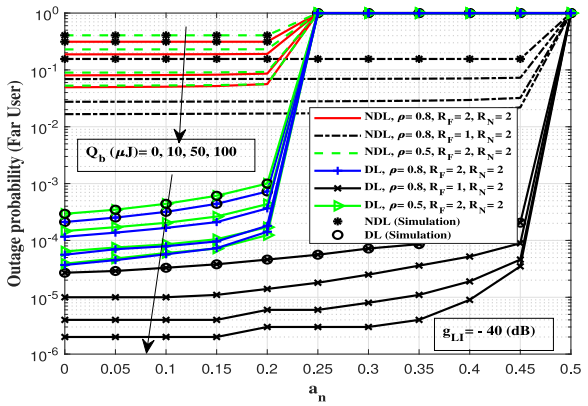

FIGURE 9. Outage probability of D_F versus a_N without the DL and with the DL using MRC.

results confirm the correctness of the derived analytical expressions. Let $\mathbb{E}[|h_{LI}|^2] = -40$ (dB) and $P_s = 20$ (dBm). When the value of a_N is increased, the outage probability of D_F rises and that of D_N falls. After a threshold value $a_F = 1 - \frac{\gamma_{th_N}^{FD}}{\gamma_{th_F}^{FD}+\gamma_{th_N}^{FD}(1+\gamma_{th_F}^{FD})}$ or $a_N = \frac{\gamma_{th_N}^{FD}}{\gamma_{th_F}^{FD}+\gamma_{th_N}^{FD}(1+\gamma_{th_F}^{FD})}$ ($a_N = 0.2$ for $R_F = 2$, $R_N = 2$, and $a_N = 0.43$ for $R_F = 1$ and $R_N = 2$), the outage probability of D_N increases with increasing a_N. This is because, at this threshold value, the SINR at D_N to decode the D_F symbol decreases. A further increase in a_N causes D_N outage probability to rise to 1, while for $a_N > \frac{1}{1+\gamma_{th_F}^{FD}}$, the outage remains at 1. D_F performance improves, but D_N performance deteriorates with increasing levels of Q_b and ρ, as predicted.

Let $\mathbb{E}|h_{LI}|^2 = -40$ (dB). The outage probability of D_F versus the source transmit power (P_s) (dBm) for the PSR protocol is plotted in Fig. 8 for different Q_b values for the NDL and the DL using MRC. For various Q_b values, the performance of D_F is compared for the DL and NDL linear and non-linear energy harvesting systems. The simulation results match the analytical expressions well. It is clear that D_F performs better in the DL case, and adding a small amount of battery energy Q_b to the harvested energy improves the outage performance (compared to the case where $Q_b = 0$). The improvement D_F performance is very significant at lower transmit power P_s, but because of the existence of the DL, the performance continues to improve at higher transmit power as well, unlike the NDL case. Additionally, for larger P_s values with NL-EH, the power at D_N is limited by γ_{sat}, which results in a floor in the outage probability when the DL is absent. However, the floor does not exist owing to the DL and battery energy, but diversity is lost compared to L-EH (diversity decreases by one). Therefore, compared to L-EH, battery-assisted relaying with DL is considerably more important in NL-EH.

Fig. 9 shows the relationship between the outage probability of D_F in both the cases of NDL and DL and a_N for various Q_b and ρ values as well as various R_F and R_N combinations. The simulation results confirm the correctness of the derived analytical expressions. For $P_s = 20$ dBm, it is clear from Fig. 9 that when a_N is increased, the outage probability of D_F slightly increases in both the cases of the DL and NDL, but with the DL, the outage probability is far lower than that with the NDL. After a threshold value $a_F = 1 - \frac{\gamma_{th_N}^{FD}}{\gamma_{th_F}^{FD}+\gamma_{th_N}^{FD}(1+\gamma_{th_F}^{FD})}$ or $a_N = \frac{\gamma_{th_N}^{FD}}{\gamma_{th_F}^{FD}+\gamma_{th_N}^{FD}(1+\gamma_{th_F}^{FD})}$ ($a_N = 0.2$ for $R_F = 2$, $R_N = 2$, and a threshold value of $a_N = 0.45$ for $R_F = 1$ and $R_N = 2$), the outage probability of D_F increases with increasing a_N. During the IT phase after $a_N = \frac{\gamma_{th_N}^{FD}}{\gamma_{th_F}^{FD}+\gamma_{th_N}^{FD}(1+\gamma_{th_F}^{FD})}$, the SINR to decode D_F symbols drops, a further rise in a_N causes an increase in the outage probability. In addition, D_F performance gets better with the DL.

Let $\mathbb{E}[|h_{LI}|^2] = -40$ dB and $Q_b = 0(\mu J)$. Fig. 10 illustrates the changes in the outage probability of D_N and D_F for different values of d_{SN} and d_{SF} versus the source transmit power P_s (dBm). The results provide new insights into the performance of the system. The outage probability of D_N increases with an increase in d_{SN}, while the outage probability of D_F increases with an increase in d_{SF}. Furthermore, the positioning of D_N significantly impacts the outage performance of both D_N and D_F. These findings indicate that the analytical model can measure outages and other performance metrics by adjusting the

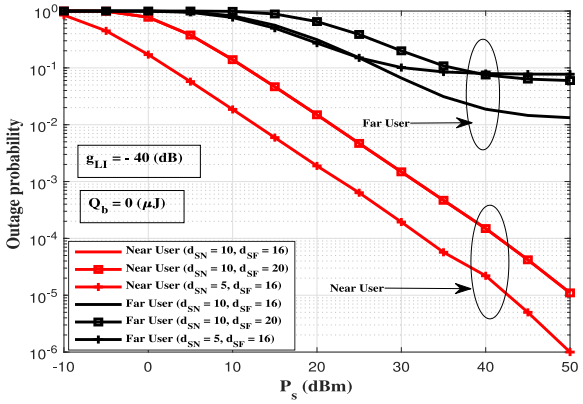

FIGURE 10. Outage probability of D_N and D_F versus the source transmit power at different node distances without the DL.

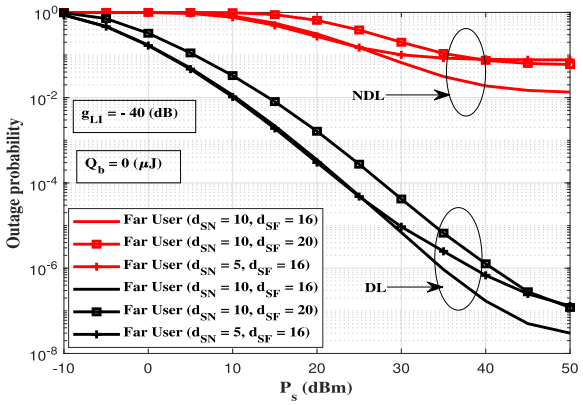

FIGURE 11. Outage probability of D_F versus the source transmit power at different node distances without the DL and with the DL using MRC.

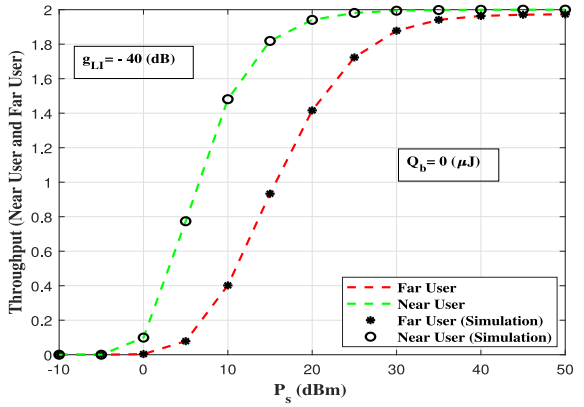

FIGURE 12. Throughput of D_F and D_N versus the source transmit power without the DL.

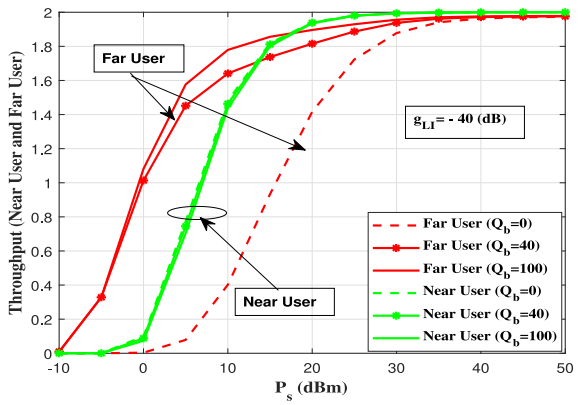

FIGURE 13. Throughput of D_F and D_N versus the source transmit power without the DL.

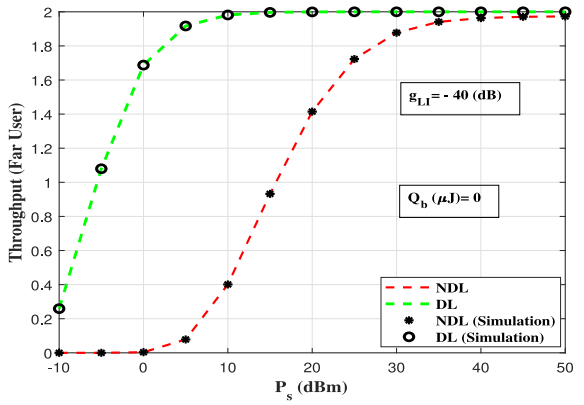

FIGURE 14. Throughput of D_F versus the source transmit power without the DL and with the DL using MRC.

node placements. Fig. 11 shows the variation in the outage probability of D_F, with both the DL and the NDL, as D_N and D_F are moved for different values of d_{SN} and d_{SF}. Changes in the distance between nodes result in D_F outage probability changes. These results highlight the potential of the analytical model to detect outages and other metrics by adjusting the placement of nodes.

Fig. 12 and Fig. 13 show the throughput of D_N and D_F versus the source transmit power P_s (dBm) considering the PSR protocol. The simulation results confirm the correctness of the derived analytical expressions. Let $\mathbb{E}|h_{LI}|^2 = -40$ (dB). Since D_N is expected to decode $D_F's$ message first and also transmit the information to D_F while harvesting sufficient energy, the $D_N's$ throughput is better than D_F at low transmit power and 0 Q_b value because D_N lacks the energy to ensure that D_F is not experiencing an outage. But as the value of Q_b increases, the throughput of D_F is better than D_N. At high transmit powers, a floor in the throughput exists due to γ_{sat}.

The throughput performance of D_F for both the cases (NDL and DL) is compared for different values of Q_b in Fig. 14 and Fig. 15. Let $\mathbb{E}|h_{LI}|^2 = -40$ (dB). The simulation results confirm the correctness of the derived analytical expressions. With the DL, D_F performs better and almost doubles the throughput. Additionally, an increase in battery energy significantly improves throughput at low transmit powers for both cases, although it has little impact at high transmit powers. When P_s is high, the DL becomes sufficiently strong for the chosen target rate. It should be noted that the γ_{sat} results in a floor when there is NDL.

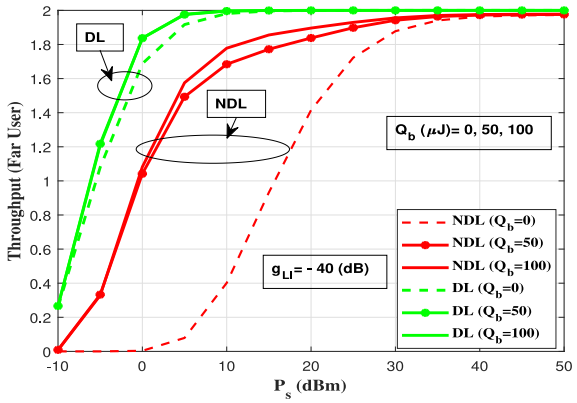

FIGURE 15. Throughput of D_F versus the source transmit power without the DL and with the DL using MRC.

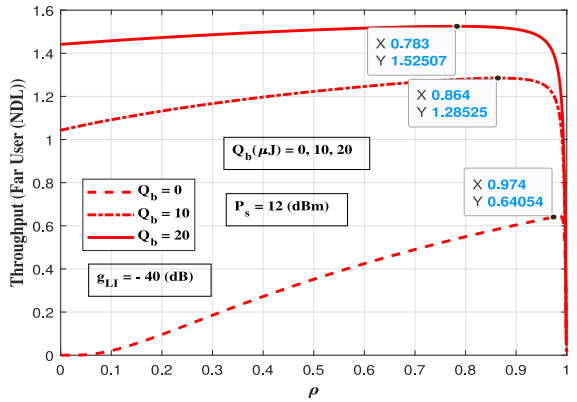

FIGURE 16. Throughput of D_F versus the energy harvesting parameter ρ without the DL.

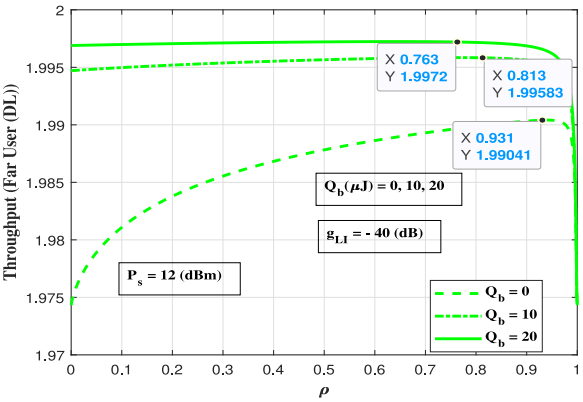

FIGURE 17. Throughput of D_F versus the energy harvesting parameter ρ with the DL using MRC.

For the range of the power splitting parameter ρ, Fig. 16 and Fig. 17 demonstrate the change in the throughput of D_F for both the scenarios of the DL and NDL for various levels of Q_b. Let $\mathbb{E}|h_{LI}|^2 = -40$ (dB) and $P_s = 12$ (dBm). The throughput is concave with respect to ρ, which means an optimal value of ρ maximizes the throughput. The optimal values of ρ are marked. D_F performs better in the DL scenario than in the NDL scenario.

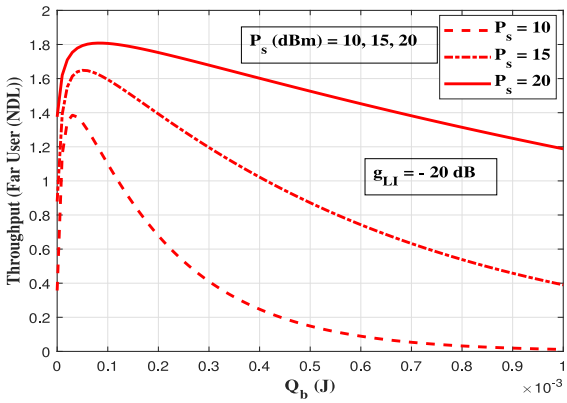

FIGURE 18. Throughput of D_F versus the battery energy Q_b without the DL.

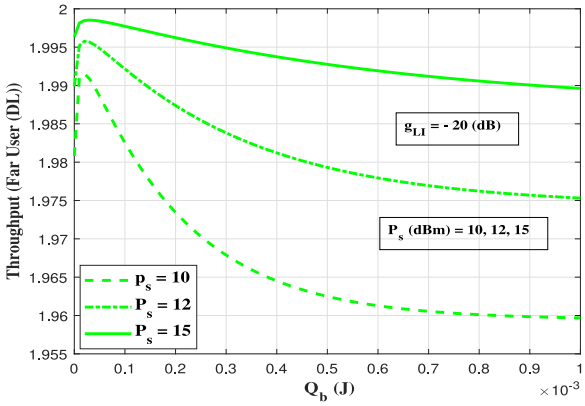

FIGURE 19. Throughput of D_F versus the battery energy Q_b with the DL using MRC.

For the range of the battery energy Q_b, Fig. 18 and Fig. 19 demonstrate the change in the throughput of D_F for both scenarios of the DL and NDL for different values of P_s. Let $\mathbb{E}|h_{LI}|^2 = -20$ (dB). A certain value of Q_b optimises throughput. Thus, there is an operational range $[0, Q_b{}^*]$ where increasing Q_b results in higher throughput. When Q_b increases beyond this value, the throughput falls due to increasing residual self-loop interference levels. It is clear that compared to the scenario when there is the NDL, using the DL results in lower battery energy needed for the desired throughput. It is evident that a single value $(Q_b{}^*, \rho^*)$ exists that maximises the throughput for a desired D_N target throughput.

Fig. 20 shows the relationship between the system's energy efficiency and the source transmit power P_s (dBm) for different Q_b and g_{LI} values. The curves illustrate that the source transmit power affects the system's energy efficiency in the DL and NDL scenarios. When the source transmit power is reduced, energy efficiency increases. On the other hand, energy efficiency performance decreases gradually as P_s increases. All the curves are plotted for various values of Q_b and g_{LI}, and the PS EH parameter is almost at its optimum value. It has been observed that the LI has a noticeable impact on energy efficiency. When the LI value

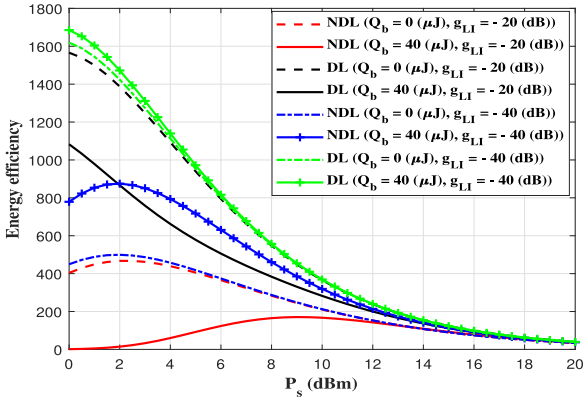

FIGURE 20. System energy efficiency versus the source transmit power for different Q_b and g_{LI} values without the DL and with the DL using MRC.

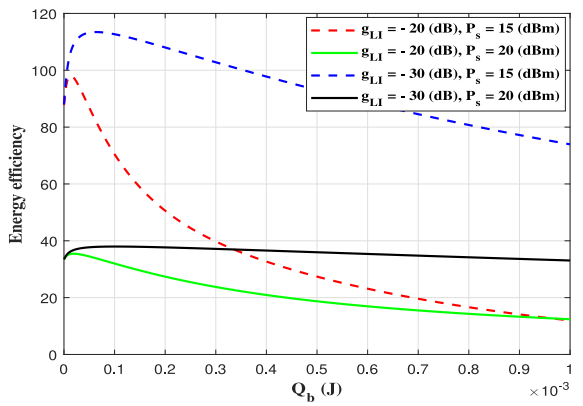

FIGURE 21. System energy efficiency versus the battery energy Q_b for different P_s and g_{LI} values without the DL.

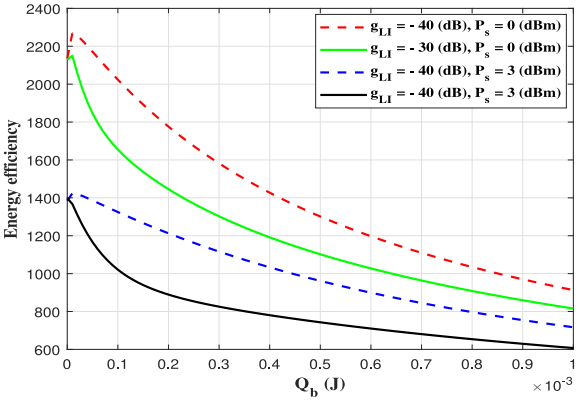

FIGURE 22. System energy efficiency versus the battery energy Q_b for different P_s and g_{LI} values with the DL using MRC.

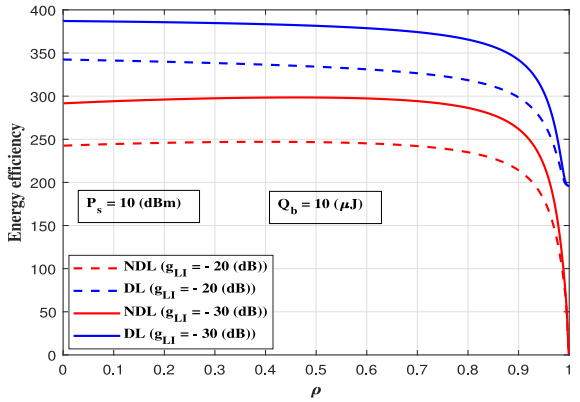

FIGURE 23. System energy efficiency versus the energy harvesting parameter ρ for different g_{LI} values without the DL and with the DL using MRC.

decreases, energy efficiency increases noticeably. The DL performance is superior as compared to the NDL.

Fig. 21 and Fig. 22 show the relationship between the energy efficiency and Q_b for different values of P_s and g_{LI}. The plots illustrate all curves with $R_N = R_F = 2$ (BPCU), while the PS EH parameter is adjusted to its optimal value. At first, D_N contributes most to energy efficiency when no battery energy is supplied (the battery energy aids throughput increase at D_F). The system's energy efficiency rises with increasing Q_b because D_F throughput increases. There is, however, a particular value of Q_b over which the energy efficiency begins to decline. This is a result of LI being present at D_N. The LI rises in tandem with the increasing Q_b, which makes it impossible to decode D_F symbols at D_N. As a result, D_F throughput declines. Both LI and P_s have a noticeable impact on the energy efficiency of the system.

Fig. 23 shows the relationship between the system's energy efficiency and the energy harvesting parameter ρ for different g_{LI} values. Let $P_s = 10$ (dBm), $Q_b = 10(\mu J)$ and $R_N = R_F = 2$ (BPCU). No energy is captured D_N with PS at $\rho = 0$, resulting in the negligible throughput of D_F. Increasing ρ further leads to an improvement in D_F throughput. Likewise, IT does not occur when $\rho = 1$, causing both the throughput and energy efficiency to drop. Additionally, energy efficiency drops significantly at high LI levels. Therefore, optimising Q_b and ρ is necessary to significantly improve and optimize the system's throughput and energy efficiency.

In Fig. 24, we display the variation in outage probability of D_F in the NDL and DL cases versus P_{sat} for $P_s = 20$ (dBm), $R_N = R_F = 1$ bpcu, and different levels of Q_b. Let $\mathbb{E}|h_{LI}|^2 = -40$ (dB). The outage probability for NL-EH improves noticeably and approaches that of the L-EH case as P_{sat} increases. Also, the performance of D_F with the NDL is inferior to that of the DL scenario. The performance becomes better with increasing levels of Q_b.

V. CONCLUSION

In specific scenarios, it may be necessary to utilize an adjacent IoT node to enhance communication range or reliability with a distant node. EH technology is a viable solution to ensure the relaying IoT node meets strict lifetime constraints. This work explores the performance of the cooperative relaying-based NOMA that employs SWIPT and battery-assisted NL-EH in two scenarios: with and without the DL. The FD mode is used along with the PSR protocol. Channels are modelled using Rayleigh fading, and the DF mechanism with imperfect successive interference

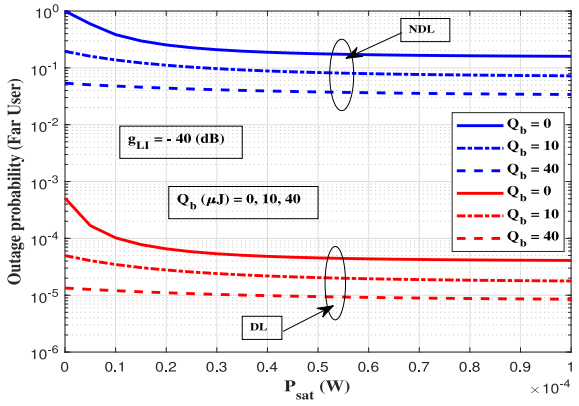

FIGURE 24. Outage probability of D_F versus saturated power P_{sat}.

cancellation (i-SIC) is used at the NU, acting as a relay. The DL at the FU is evaluated in two scenarios: as an optimal combination to the signal from the NU and as an interfering link to the signal from the NU. Closed-form expressions for the NU and FU outage probability and throughput have been derived by combining the PSR protocol with NL-EH. We established the diversity order by deriving high SNR approximation equations of the NU and FU outage probability in NDL and DL scenarios. We established that, in contrast to L-EH, NL-EH incurs a diversity loss, which makes combining with the DL essential for increasing throughput and minimizing battery energy usage. We showed that the performance of the FU is significantly enhanced by adding a small quantity of battery energy to the harvested energy at the NU, which acts as a relay. We have demonstrated that the residual interference generated by i-SIC significantly impacts the outage probability of the NU while having a negligible effect on the performance of the FU. Additionally, we have found that the performance degrades in the context of IDL. We have formulated an equation to measure energy efficiency using the derived throughput expressions for the NDL and DL scenarios. We have also shown that selecting the optimal combination of battery energy and PS parameter is essential to achieve the highest possible throughput and energy efficiency. We explain how the system's performance is affected by the selection of energy harvesting parameter, power allocation coefficient, saturation threshold, self-loop interference, variable node distances and battery energy. Monte Carlo simulations have verified the accuracy of the resulting expressions.

APPENDIX A
PROOF OF LEMMA 2

From (24), I_1 is expressed as

$$I_1 = \int_{\beta_1}^{\phi_1} \lambda_{SN} e^{-\lambda_{SN} x} e^{-\frac{\lambda_{NF} C_l \gamma_{th_F}^{FD}}{\eta \rho x \gamma_s + \gamma_b}} dx. \tag{A.1}$$

We use a linear approximation of the exponential term ($e^{ax} \approx 1 + ax$) for high γ_s in (A.1) to get

$$I_1 = \int_{\beta_1}^{\phi_1} \lambda_{SN} e^{-\lambda_{SN} x} \frac{\eta \rho x \gamma_s + \gamma_b}{\eta \rho x \gamma_s + \gamma_b + \lambda_{NF} C_l \gamma_{th_F}^{FD}} dx. \tag{A.2}$$

After some mathematical steps, (A.2) can be written as

$$I_1 = \underbrace{\int_{\beta_1}^{\phi_1} \lambda_{SN} e^{-\lambda_{SN} x} dx}_{I_{11}} - \underbrace{\int_{\beta_1}^{\phi_1} \lambda_{SN} e^{-\lambda_{SN} x} \frac{\lambda_{NF} C_l \gamma_{th_F}^{FD}}{\eta \rho x \gamma_s + \gamma_b + \lambda_{NF} C_l \gamma_{th_F}^{FD}} dx}_{I_{12}}, \tag{A.3}$$

where I_{11} and I_{12} are given by

$$I_{11} = \left(e^{-\lambda_{SN}\beta_1} - e^{-\lambda_{SN}\phi_1}\right),$$

and

$$I_{12} = \frac{\lambda_{NF}\lambda_{SN} C_l \gamma_{th_F}^{FD}}{\eta \rho \gamma_s} \times \left[e^{\mu_1 \lambda_{SN}} \begin{Bmatrix} E_i(-(\mu_1+\phi_1)\lambda_{SN}) \\ -E_i(-(\mu_1+\beta_1)\lambda_{SN}) \end{Bmatrix} \right]$$

is obtained from [54, 3.352.3]. Substituting the values of I_{11} and I_{12} in (A.3), I_1 is obtained. Now I_2 is expressed as

$$I_2 = e^{-\lambda_{SN} \max(\phi_2, \beta_2) - \frac{\lambda_{NF} \gamma_{th_F}^{FD}}{\eta \gamma_{sat} + \gamma_b}}. \tag{A.4}$$

Substituting these values of I_1 and I_2 in (24), the outage probability of the FU with NDL is obtained as (25).

APPENDIX B

Using (31), the outage probability of the FU with the DL can be written as

$$P_{D_F,dir}^{FD} = I_1 + I_2 + I_3. \tag{B.1}$$

Now I_1 is expressed as

$$I_1 = \left(1 - e^{-\lambda_{SN}\beta_1}\right)\left(1 - e^{-\lambda_{SF} L_1}\right), \tag{B.2}$$

and I_2 is calculated as

$$I_2 = \left(e^{-\lambda_{SN}\beta_1} - e^{-\lambda_{SN}\phi_1}\right)\left(1 - e^{-\lambda_{SF} L_1}\right) - \lambda_{SN}\lambda_{SF} \times \int_{\beta_1}^{\phi_1} \int_0^{L_1} e^{-\lambda_{SN} x} e^{-\lambda_{SF} z} \times e^{-\lambda_{NF}\left(\frac{\gamma_{th_F}^{FD} C_l (z\gamma_s a_N C_l + C_l) - z\gamma_s a_F C_l^2}{(\eta \rho x \gamma_s + \gamma_b)(z\gamma_s a_N C_l + C_l)}\right)} dx dz. \tag{B.3}$$

We use a linear approximation of the exponential term ($e^{ax} \approx 1 + ax$) for high γ_s in (B.3) to get

$$I_2 = \left(e^{-\lambda_{SN}\beta_1} - e^{-\lambda_{SN}\phi_1}\right)\left(1 - e^{-\lambda_{SF} L_1}\right) - \lambda_{SN}\lambda_{SF} \times \int_{\beta_1}^{\phi_1} \int_0^{L_1} e^{-\lambda_{SN} x} e^{-\lambda_{SF} z} \lambda_{NF}$$

$$\times\left(\frac{\gamma_{th_F}^{FD}C_l(A)-B}{(\eta\rho x\gamma_s+\gamma_b)(A)+\lambda_{NF}\left(\gamma_{th_F}^{FD}C_l(A)-B\right)}\right)dxdz \tag{B.4}$$

where $A=(z\gamma_s a_N C_l+C_l)$ and $B=z\gamma_s a_F C_l^2$. After some mathematical steps, I_2 is expressed as

$$I_2=\lambda_{SN}\lambda_{SF}\int_{\beta_1}^{\phi_1}\int_0^{L_1}e^{-\lambda_{SN}x}e^{-\lambda_{SF}z}\frac{\lambda_{NF}}{\eta\rho\gamma_s A}\times\left(\frac{\gamma_{th_F}^{FD}C_l(A)-B}{\left(x+\frac{\gamma_b}{\eta\rho\gamma_s}\right)+\frac{\lambda_{NF}}{\eta\rho\gamma_s A}\left(\gamma_{th_F}^{FD}C_l(A)-B\right)}\right)dxdz. \tag{B.5}$$

Furthermore, using [54, 3.352.3], I_2 is given by

$$\begin{aligned}I_2=\lambda_{SN}\lambda_{SF}\int_0^{L_1}&\frac{\lambda_{NF}}{\eta\rho\gamma_s A}\left(\gamma_{th_F}^{FD}C_lA-B\right)\\&\times e^{\lambda_{SN}\left(\frac{\gamma_b}{\eta\rho\gamma_s}+\frac{\lambda_{NF}}{\eta\rho\gamma_s A}\left(\gamma_{th_F}^{FD}C_lA-B\right)\right)-\lambda_{SF}z}\\&\times\left[E_1\left\{\lambda_{SN}\left(\beta_1+\frac{\gamma_b}{\eta\rho\gamma_s}+\frac{\lambda_{NF}}{\eta\rho\gamma_s A}\left(\gamma_{th_F}^{FD}C_lA-B\right)\right)\right\}\right.\\&\left.-E_1\left\{\lambda_{SN}\left(\phi_1+\frac{\gamma_b}{\eta\rho\gamma_s}+\frac{\lambda_{NF}}{\eta\rho\gamma_s A}\left(\gamma_{th_F}^{FD}C_lA-B\right)\right)\right\}\right]dz.\end{aligned} \tag{B.6}$$

It is difficult to solve the integral in (B.6), but at high γ_s, we can use the approximation $e^u E_1(u)\approx 1/u$, and after some mathematical steps, (B.6) can be written as

$$\begin{aligned}I_2=&e^{-\lambda_{SN}\beta_1}\left(1-e^{-\lambda_{SF}L_1}\right)-\lambda_{SF}\left(\beta_1+\frac{\gamma_b}{\eta\rho\gamma_s}\right)e^{-\lambda_{SN}\beta_1}\\&\times\int_0^{L_1}\frac{e^{-\lambda_{SF}z}}{\beta_1+\frac{\gamma_b}{\eta\rho\gamma_s}+\frac{\lambda_{NF}\left(\gamma_{th_F}^{FD}C_lA-B\right)}{\eta\rho\gamma_s A}}dz\\&-e^{-\lambda_{SN}\phi_1}\left(1-e^{-\lambda_{SF}L_1}\right)\\&+\int_0^{L_1}\frac{e^{-\lambda_{SF}z}}{\phi_1+\frac{\gamma_b}{\eta\rho\gamma_s}+\frac{\lambda_{NF}\left(\gamma_{th_F}^{FD}C_lA-B\right)}{\eta\rho\gamma_s A}}dz.\end{aligned} \tag{B.7}$$

After some mathematical rearrangements in (B.7) and using [54, 3.352.3], I_2 is obtained. Similarly, I_3 is calculated as

$$I_3=\underbrace{(X>max(\phi_2,\beta_2))}_{I_{31}}\underbrace{(Y<A_2,Z<L_1)}_{I_{32}} \tag{B.8}$$

where I_{31} is given by

$$I_{31}=e^{-\lambda_{SN}max(\phi_2,\beta_2)} \tag{B.9}$$

and I_{32} is given by

$$I_{32}=\left(1-e^{-\lambda_{SF}L_1}\right)-\lambda_{SF}\int_0^{L_1}e^{-\lambda_{SF}z}\times e^{-\frac{\lambda_{NF}\left(\gamma_{th_F}^{FD}(z\gamma_s a_N+1)-z\gamma_s a_F\right)}{(\eta\gamma_{sat}+\gamma_b)(z\gamma_s a_N+1)}}dz. \tag{B.10}$$

The quantity I_{32} is obtained by a similar method for I_2. Substituting I_{31} and I_{32} in (B.8), I_3 is obtained.

APPENDIX C

From (38), $\hat{I}_1$ and $\hat{I}_2$ are calculated as

$$\hat{I}_1=\lambda_{SN}\lambda_{SF}\int_0^{\infty}\int_{\beta_1}^{\phi_1}e^{-\lambda_{SN}x}e^{-\frac{b_1(z)}{x}}e^{-\lambda_{SF}z}dxdz \tag{C.1}$$

where

$$b_1(z)=\frac{\lambda_{NF}\gamma_{th_F}^{FD}C_l(\delta z\gamma_s+1)-\gamma_b}{\eta\rho\gamma_s}.$$

Now $\hat{I}_1$ can be determined by using the Maclaurin series expansion for the term $e^{-b_1(z)/x}$ and further simplifying using [54, 3.352.2] and [54, 3.353.1], as

$$\begin{aligned}\hat{I}_1=&\lambda_{SN}\lambda_{SF}\int_0^{\infty}P_1e^{-\lambda_{SF}z}dz-\lambda_{SN}\lambda_{SF}P_2\\&\times\int_0^{\infty}b_1(z)e^{-\lambda_{SF}z}dz+\lambda_{SN}\lambda_{SF}\sum_{n=2}^{\infty}\frac{-1^n}{n!}P_4\\&\times\int_0^{\infty}(b_1(z))^ne^{-\lambda_{SF}z}dz\end{aligned} \tag{C.2}$$

which can be rewritten as

$$\begin{aligned}\hat{I}_1=&\lambda_{SN}P_1-\lambda_{SN}\lambda_{SF}P_2\left[P_3\delta\gamma_s\int_0^{\infty}ze^{-\lambda_{SF}z}dz+P_3\right.\\&\left.\times\int_0^{\infty}e^{-\lambda_{SF}z}dz\right]+\int_0^{\infty}b_1(z)e^{-\lambda_{SF}}zdz+\lambda_{SN}\lambda_{SF}\\&\times\sum_{n=2}^{\infty}\frac{-1^n}{n!}P_4\int_0^{\infty}(b_1(z))^ne^{-\lambda_{SF}z}dz.\end{aligned} \tag{C.3}$$

Solving (C.3), $\hat{I}_1$ given in (39) is obtained. Now, $\hat{I}_2$ is calculated as

$$\hat{I}_2=\lambda_{SN}\lambda_{SF}\int_0^{\infty}\int_{\max(\phi_2,\beta_2)}^{\infty}e^{-\lambda_{SN}x}e^{-b_2(z)}e^{-\lambda_{SF}z}dxdz \tag{C.4}$$

where

$$b_2(z)=\frac{\lambda_{NF}\gamma_{th_F}^{FD}(\delta z\gamma_s+1)}{\eta\gamma_{sat}+\gamma_b}.$$

Using the same approach as in $\hat{I}_1$, $\hat{I}_2$ is given as

$$\begin{aligned}\hat{I}_2=&\lambda_{SN}\lambda_{SF}\left[\frac{1}{\lambda_{SF}}-\left\{P_5\delta\gamma_s\int_0^{\infty}ze^{-\lambda_{SF}z}dz+P_5\right.\right.\\&\left.\left.\times\int_0^{\infty}e^{-\lambda_{SF}z}dz\right\}+\sum_{n=2}^{\infty}\frac{-1^n}{n!}\int_0^{\infty}(b_2(z))^ne^{-\lambda_{SF}z}dz\right]\\&\times\int_{\max(\phi_2,\beta_2)}^{\infty}e^{-\lambda_{SN}x}dx.\end{aligned} \tag{C.5}$$

Solving (C.5), $\hat{I}_2$ given in (40) is obtained.

REFERENCES

[1] Z. Ding et al., "Application of non-orthogonal multiple access in LTE and 5G networks," *IEEE Commun. Mag.*, vol. 55, no. 2, pp. 185–191, Feb. 2017.

[2] L. Dai, B. Wang, Y. Yuan, S. Han, I. Chih-lin, and Z. Wang, "Non-orthogonal multiple access for 5G: Solutions, challenges, opportunities, and future research trends," *IEEE Commun. Mag.*, vol. 53, no. 9, pp. 74–81, Sep. 2015.

[3] S. M. R. Islam, N. Avazov, O. A. Dobre, and K.-S. Kwak, "Power-domain non-orthogonal multiple access (NOMA) in 5G systems: Potentials and challenges," *IEEE Commun. Surveys Tuts.*, vol. 19, no. 2, pp. 721–742, 2nd Quart., 2017.

[4] S. Ulukus et al., "Energy harvesting wireless communications: A review of recent advances," *IEEE J. Sel. Areas Commun.*, vol. 33, no. 3, pp. 360–381, Mar. 2015.

[5] M. Shafi et al., "5G: A tutorial overview of standards, trials, challenges, deployment, and practice," *IEEE J. Sel. Areas Commun.*, vol. 35, no. 6, pp. 1201–1221, Jun. 2017.

[6] D. Korpi, L. Anttila, V. Syrjala, and M. Valkama, "Widely linear digital self-interference cancellation in the direct-conversion full-duplex transceiver," *IEEE J. Sel. Areas Commun.*, vol. 32, no. 9, pp. 1674–1687, Sep. 2014.

[7] X. Shao, C. Yang, D. Chen, N. Zhao, and F. R. Yu, "Dynamic IoT device clustering and energy management with hybrid NOMA systems," *IEEE Trans. Ind. Informat.*, vol. 14, no. 10, pp. 4622–4630, Oct. 2018.

[8] Z. Ding, M. Peng, and H. V. Poor, "Cooperative non-orthogonal multiple access in 5G systems," *IEEE Commun. Lett.*, vol. 19, no. 8, pp. 1462–1465, Aug. 2015.

[9] Y. Liu, Z. Ding, M. Elkashlan, and H. V. Poor, "Cooperative nonorthogonal multiple access with simultaneous wireless information and power transfer," *IEEE J. Sel. Areas Commun.*, vol. 34, no. 4, pp. 938–953, Apr. 2016.

[10] C. Zhong and Z. Zhang, "Non-orthogonal multiple access with cooperative full-duplex relaying," *IEEE Commun. Lett.*, vol. 20, no. 12, pp. 2478–2481, Dec. 2016.

[11] Y. He, X. Cheng, W. Peng, and G. L. Stuber, "A survey of energy harvesting communications: Models and optimal offline policies," *IEEE Commun. Mag.*, vol. 53, no. 6, pp. 79–85, Jun. 2015.

[12] B. Clerckx, R. Zhang, R. Schober, D. W. K. Ng, D. I. Kim, and H. V. Poor, "Fundamentals of wireless information and power transfer: From RF energy harvester models to signal and system designs," *IEEE J. Sel. Areas Commun.*, vol. 37, no. 1, pp. 4–33, Jan. 2019.

[13] A. A. Nasir, X. Zhou, S. Durrani, and R. A. Kennedy, "Relaying protocols for wireless energy harvesting and information processing," *IEEE Trans. Wireless Commun.*, vol. 12, no. 7, pp. 3622–3636, Jul. 2013.

[14] Z. Zhou, M. Peng, Z. Zhao, W. Wang, and R. S. Blum, "Wireless-powered cooperative communications: Power-splitting relaying with energy accumulation," *IEEE J. Sel. Areas Commun.*, vol. 34, no. 4, pp. 969–982, Apr. 2016.

[15] S. Modem and S. Prakriya, "Performance of EH protocols in two-hop networks with a battery-assisted EH relay," *IEEE Trans. Veh. Technol.*, vol. 67, no. 10, pp. 10022–10026, Oct. 2018.

[16] Y. Alsaba, C. Y. Leow, and S. K. Abdul Rahim, "Full-duplex cooperative non-orthogonal multiple access with beamforming and energy harvesting," *IEEE Access*, vol. 6, pp. 19726–19738, 2018.

[17] Y. Yuan, Y. Xu, Z. Yang, P. Xu, and Z. Ding, "Energy efficiency optimization in full-duplex user-aided cooperative SWIPT NOMA systems," *IEEE Trans. Commun.*, vol. 67, no. 8, pp. 5753–5767, Aug. 2019.

[18] C. Guo, L. Zhao, C. Feng, Z. Ding, and H.-H. Chen, "Energy harvesting enabled NOMA systems with full-duplex relaying," *IEEE Trans. Veh. Technol.*, vol. 68, no. 7, pp. 7179–7183, Jul. 2019.

[19] P. Deng, B. Wang, W. Wu, and T. Guo, "Transmitter design in MISO-NOMA system with wireless-power supply," *IEEE Commun. Lett.*, vol. 22, no. 4, pp. 844–847, Apr. 2018.

[20] H. Huang and M. Zhu, "Energy efficiency maximization design for full-duplex cooperative NOMA systems with SWIPT," *IEEE Access*, vol. 7, pp. 20442–20451, 2019.

[21] P. D. Diamantoulakis, K. N. Pappi, Z. Ding, and G. K. Karagiannidis, "Wireless-powered communications with non-orthogonal multiple access," *IEEE Trans. Wireless Commun.*, vol. 15, no. 12, pp. 8422–8436, Dec. 2016.

[22] W. Lu, Y. Ding, Y. Gao, Y. Chen, N. Zhao, Z. Ding, and A. Nallanathan, "Secure NOMA-based UAV-MEC network towards a flying eavesdropper," *IEEE Trans. Commun.*, vol. 70, no. 5, pp. 3364–3376, May 2022.

[23] Y. Wu, Y. Song, T. Wang, L. Qian, and T. Q. S. Quek, "Non-orthogonal multiple access assisted federated learning via wireless power transfer: A cost-efficient approach," *IEEE Trans. Commun.*, vol. 70, no. 4, pp. 2853–2869, Apr. 2022.

[24] L. Bariah, S. Muhaidat, and A. Al-Dweik, "Error probability analysis of NOMA-based relay networks with SWIPT," *IEEE Commun. Lett.*, vol. 23, no. 7, pp. 1223–1226, Jul. 2019.

[25] E. Boshkovska, D. W. K. Ng, N. Zlatanov, and R. Schober, "Practical non-linear energy harvesting model and resource allocation for SWIPT systems," *IEEE Commun. Lett.*, vol. 19, no. 12, pp. 2082–2085, Dec. 2015.

[26] K. Agrawal, S. Prakriya, and M. F. Flanagan, "NOMA with battery-assisted energy harvesting full-duplex relay," *IEEE Trans. Veh. Technol.*, vol. 69, no. 11, pp. 13952–13957, Nov. 2020.

[27] L. Ma, E. Li, and Q. Yang, "On the performance of full-duplex cooperative NOMA with non-linear EH," *IEEE Access*, vol. 9, pp. 145968–145976, 2021.

[28] M. Min, L. Xiao, Y. Chen, P. Cheng, D. Wu, and W. Zhuang, "Learning based computation offloading for IoT devices with energy harvesting," *IEEE Trans. Veh. Technol.*, vol. 68, no. 2, pp. 1930–1941, Feb. 2019.

[29] A. Alrabea, O. A. Alzubi, and O. Alzubi, "A task-based model for minimizing energy consumption in WSNs," *Energy Syst.*, vol. 13, pp. 671–688, Aug. 2022.

[30] R. Jain, V. Goel, J. K. Rekhi, and J. A. Alzubi, "IoT based green building: Towards an energy-efficient future," *Green Build. Manag. Smart Automat.*, vol. 68, no. 2, pp. 184–207, 2019.

[31] Y. Khawaja, I. Qiqieh, J. Alzubi, O. Alzubi, A. Allahham, and D. Giaouris, "Design of cost-based sizing and energy management framework for standalone microgrid using reinforcement learning," *Sol. Energy*, vol. 251, pp. 249–260, Feb. 2023.

[32] W. Lu et al., "SWIPT cooperative spectrum sharing for 6G-enabled cognitive IoT network," *IEEE Int. Things J.*, vol. 8, no. 20, pp. 15070–15080, Oct. 2021.

[33] I. Krikidis, S. Timotheou, S. Nikolaou, G. Zheng, D. W. K. Ng, and R. Schober, "Simultaneous wireless information and power transfer in modern communication systems," *IEEE Commun. Mag.*, vol. 52, no. 11, pp. 104–110, Nov. 2014.

[34] R. Morsi, D. S. Michalopoulos, and R. Schober, "Performance analysis of near-optimal energy buffer aided wireless powered communication," *IEEE Trans. Wireless Commun.*, vol. 17, no. 2, pp. 863–881, Feb. 2018.

[35] N. Li, M. Xiao, and L. K. Rasmussen, "Optimized cooperative multiple access in industrial cognitive networks," *IEEE Trans. Ind. Informat.*, vol. 14, no. 6, pp. 2666–2676, Jun. 2018.

[36] X. Pei, H. Yu, X. Wang, Y. Chen, M. Wen, and Y.-C. Wu, "NOMA-based pervasive edge computing: Secure power allocation for IoV," *IEEE Trans. Ind. Informat.*, vol. 17, no. 7, pp. 5021–5030, Jul. 2021.

[37] A. Sabharwal, P. Schniter, D. Guo, D. W. Bliss, S. Rangarajan, and R. Wichman, "In-band full-duplex wireless: Challenges and opportunities," *IEEE J. Sel. Areas Commun.*, vol. 32, no. 9, pp. 1637–1652, Sep. 2014.

[38] L. Dai, B. Wang, Z. Ding, Z. Wang, S. Chen, and L. Hanzo, "A survey of non-orthogonal multiple access for 5G," *IEEE Commun. Surveys Tuts.*, vol. 20, no. 3, pp. 2294–2323, 3rd Quart., 2018.

[39] K. Agrawal, S. Prakriya, and M. F. Flanagan, "Optimization of SWIPT with battery-assisted energy harvesting full-duplex relays," *IEEE Trans. Green Commun. Netw.*, vol. 5, no. 1, pp. 243–260, Mar. 2021.

[40] T. Riihonen, S. Werner, and R. Wichman,"Mitigation of loopback self-interference in full-duplex MIMO relays," *IEEE Trans. Signal Process.*, vol. 59, no. 12, pp. 5983–5993, Dec. 2011.

[41] G. Liu, F. R. Yu, H. Ji, V. C. M. Leung, and X. Li, "In-band full-duplex relaying: A survey, research issues and challenges," *IEEE Commun. Surveys Tuts.*, vol. 17, no. 2, pp. 500–524, Jan. 2015.

[42] D. Bharadia, E. McMilin, and S. Katti, "Full duplex radios," *ACM SIGCOMM Comput. Commun. Rev.*, vol. 43, no. 4, pp. 375–386, Aug. 2013, doi: 10.1145/2534169.2486033.

[43] D. Wang, R. Zhang, X. Cheng, and L. Yang, "Capacity-enhancing full-duplex relay networks based on power-splitting (PS) SWIPT," *IEEE Trans. Veh. Technol.*, vol. 66, no. 6, pp. 5446–5450, Jun. 2017.

[44] H. Liu, K. J. Kim, K. S. Kwak, and H. V. Poor, "Power splitting-based SWIPT with decode-and-forward full-duplex relaying," *IEEE Trans. Wireless Commun.*, vol. 15, no. 11, pp. 7561–7577, Nov. 2016.

[45] A. J. Williams, M. F. Torquato, I. M. Cameron, A. A. Fahmy, and J. Sienz, "Survey of energy harvesting technologies for wireless sensor networks," *IEEE Access*, vol. 9, pp. 77493–77510, 2021.

[46] R. Zhang, A. Nayak, and J. Yu, "Sleep scheduling in energy harvesting wireless body area networks," *IEEE Commun. Mag.*, vol. 57, no. 2, pp. 95–101, Feb. 2019.

[47] N. Li, M. Xiao, L. K. Rasmussen, X. Hu, and V. C. M. Leung, "On resource allocation of cooperative multiple access strategy in energy-efficient Industrial Internet of Things," *IEEE Trans. Ind. Informat.*, vol. 17, no. 2, pp. 1069–1078, Feb. 2021.
[48] S. Pejoski, Z. Hadzi-Velkov, and R. Schober, "Optimal power and time allocation for WPCNs with piece-wise linear EH model," *IEEE Wireless Commun. Lett.*, vol. 7, no. 3, pp. 364–367, Jun. 2018.
[49] A. El Gammal, M. Mohseni, and S. Zahedi, "Bounds on capacity and minimum energy-per-bit for AWGN relay channels," *IEEE Trans. Inf. Theory*, vol. 52, no. 4, pp. 1545–1561, Apr. 2006.
[50] D. P. M. Osorio, E. E. B. Olivo, H. Alves, J. C. S. S. Filho, and M. Latva-aho, "Exploiting the direct link in full-duplex amplify-and forward relaying networks," *IEEE Signal Process. Lett.*, vol. 22, no. 10, pp. 1766–1770, Oct. 2015.
[51] T. Riihonen, S. Werner, and R. Wichman, "Hybrid full-duplex/half-duplex relaying with transmit power adaptation," *IEEE Trans. Wireless Commun.*, vol. 10, no. 9, pp. 3074–3085, Sep. 2011.
[52] Z. Zhang, Z. Ma, M. Xiao, Z. Ding, and P. Fan, "Full-duplex device-to device aided cooperative non-orthogonal multiple access," *IEEE Trans. Veh. Technol.*, vol. 66, no. 5, pp. 4467–4471, May 2017.
[53] M. Abramowitz and I. A. Stegun, *Handbook of Mathematical Functions: With Formulas, Graphs, and Mathematical Tables*. New York, NY, USA: Dover, 1965.
[54] I. S. Gradshteyn and I. M. Ryzhik, "Table of integrals, series and products," 6th ed. New York, NY, USA: Acad. Press, 2000.
[55] X. Yue, Y. Liu, S. Kang, A. Nallanathan, and Z. Ding, "Exploiting full/half-duplex user relaying in NOMA systems," *IEEE Trans. Commun.*, vol. 66, no. 2, pp. 560–575, Feb. 2018.
[56] X. Li, J. Li, Y. Liu, Z. Ding, and A. Nallanathan, "Residual transceiver hardware impairments on cooperative NOMA networks," *IEEE Trans. Wireless Commun.*, vol. 19, no. 1, pp. 680–695, Jan. 2020.
[57] M. R. G. Aghdam, B. M. Tazehkand, and R. Abdolee, "On the performance analysis of mmWave MIMO-NOMA transmission scheme," *IEEE Trans. Veh. Technol.*, vol. 69, no. 10, pp. 11491–11500, Oct. 2020.
[58] A. A. Nasir, H. D. Tuan, T. Q. Duong, and M. Debbah, "NOMA throughput and energy efficiency in energy harvesting enabled networks," *IEEE Trans. Commun.*, vol. 67, no. 9, pp. 6499–6511, Sep. 2019.

MUDASIR BAKSHI (Graduate Student Member, IEEE) received the M.Tech. degree in electronics and communication engineering from the Jamia Millia Islamia, New Delhi, India, in 2018. He is currently pursuing the Ph.D. degree in wireless communications with the Bharti School of Telecommunication Technology and Management, Indian Institute of Technology Delhi, New Delhi, India. He qualified the GATE examination in 2016 and 2017. His research interests include NOMA, channel modeling, cooperative communications, energy harvesting, full-duplex communications, and next-generating communication technologies.

BREJESH LALL (Senior Member, IEEE) received the B.E. degree in electronics and communication engineering and the M.E. degree in signal processing from the Delhi College of Engineering, New Delhi, in 1991 and 1992, respectively, and the Ph.D. degree in signal processing from the Indian Institute of Technology (IIT) Delhi, New Delhi, in 1999. From 1997 to 2005, he was with Hughes Software Systems, where he worked in the signal processing group on source coding and PHY layer solutions for many communication technologies, such as terrestrial wireless, GEO and LEO Satellite communication systems, and satellite broadband. He joined the Department of Electrical Engineering, IIT Delhi as a Faculty Member in 2005, where he is currently a Professor. He has served as the Head of the Bharti School of Telecommunication Technology and Management, IIT Delhi, and the Coordinator of the National Cadet Corps, IIT Delhi. His research interests are broadly in signal processing, image processing, and communications, including the areas of object representation, tracking, and classification, odometry, depth map generation, representation, and rendering, vector sensor-based underwater acoustic communications, and performance issues in molecular communications.

RANJAN K. MALLIK (Fellow, IEEE) received the B.Tech. degree in electrical engineering from the Indian Institute of Technology Kanpur, Kanpur, in 1987, and the M.S. and Ph.D. degrees in electrical engineering from the University of Southern California, Los Angeles, in 1988 and 1992, respectively.

From August 1992 to November 1994, he was a Scientist with the Defence Electronics Research Laboratory, Hyderabad, India, working on missile and EW projects. From November 1994 to January 1996, he was a Faculty Member with the Department of Electronics and Electrical Communication Engineering, Indian Institute of Technology Kharagpur, Kharagpur. From January 1996 to December 1998, he was with the faculty of the Department of Electronics and Communication Engineering, Indian Institute of Technology Guwahati, Guwahati. Since December 1998, he has been with the faculty of the Department of Electrical Engineering, Indian Institute of Technology Delhi, New Delhi, where he is currently a Professor. His research interests are in diversity combining and channel modeling for wireless communications, spacetime systems, cooperative communications, multiple-access systems, power line communications, molecular communications, difference equations, and linear algebra. He is a recipient of the Hari Om Ashram Prerit Dr. Vikram Sarabhai Research Award in the field of electronics, telematics, informatics, and automation, the Shanti Swarup Bhatnagar Prize in engineering sciences, the Khosla National Award, the IEI-IEEE Award for Engineering Excellence, and the J. C. Bose Fellowship. He has served as an Area Editor and an Editor for the IEEE TRANSACTIONS ON WIRELESS COMMUNICATIONS, and as an Editor for the IEEE TRANSACTIONS ON COMMUNICATIONS. He is a member of Eta Kappa Nu, the IEEE Communications, Information Theory, and Vehicular Technology Societies, the American Mathematical Society, the International Linear Algebra Society, and the Association for Computing Machinery; a Fellow of the Indian National Academy of Engineering, the Indian National Science Academy, The National Academy of Sciences, India, Prayagraj, the Indian Academy of Sciences, Bengaluru, The World Academy of Sciences-for the advancement of science in developing countries (TWAS), The Institution of Engineering and Technology, U.K., The Institution of Electronics and Telecommunication Engineers, India, The Institution of Engineers (India) [IEI], the Asia-Pacific Artificial Intelligence Association, and the Artificial Intelligence Industry Academy; and a Life Member of the Indian Society for Technical Education.

AMIT SINGHAL (Senior Member, IEEE) received the dual degree with B.Tech. in electrical engineering and M.Tech. in information and communication technology from the Indian Institute of Technology (IIT) Delhi in 2009, and the Ph.D. degree in molecular communications from IIT Delhi in 2016. He has a total teaching experience of more than 14 years. Before joining NSUT in June 2021, he worked with JIIT Noida and Bennett University, Greater Noida. In addition to his degrees in the technical domain, he also holds a minor degree in business management with IIT Delhi in 2009. He has published several research papers in reputed journals and conferences. His areas of interest include image processing, molecular communications, next-generating communication technologies, image retrieval, theory and applications of Fourier methods.